

A MOVING-BOUNDARY MODEL OF REACTIVE SETTLING IN WASTEWATER TREATMENT

RAIMUND BÜRGER

CPMA and Departamento de Ingeniería Matemática, Facultad de Ciencias Físicas y Matemáticas, Universidad de Concepción, Casilla 160-C, Concepción, Chile

JULIO CAREAGA

Centre for Mathematical Sciences, Lund University, P.O. Box 118, S-221 00 Lund, Sweden

STEFAN DIEHL*

Centre for Mathematical Sciences, Lund University, P.O. Box 118, S-221 00 Lund, Sweden *Corresponding author: stefan.diehl@math.lth.se

ROMEL PINEDA

CPMA and Departamento de Ingeniería Matemática, Facultad de Ciencias Físicas y Matemáticas, Universidad de Concepción, Casilla 160-C, Concepción, Chile

ABSTRACT. Reactive settling is the process of sedimentation of small solid particles in a fluid with simultaneous reactions between the components of the solid and liquid phases. This process is important in sequencing batch reactors (SBRs) in wastewater treatment plants. In that application the particles are biomass (bacteria; activated sludge) and the liquid contains substrates (nitrogen, phosphorus) to be removed through reactions with the biomass. The operation of an SBR in cycles of consecutive fill, react, settle, draw, and idle stages is modeled by a system of spatially one-dimensional, nonlinear, strongly degenerate parabolic convection-diffusion-reaction equations. This system is coupled via conditions of mass conservation to transport equations on a half line, whose origin is located at a moving boundary and that model the effluent pipe. A monotone and invariant-region-preserving finite difference scheme is proposed and applied to simulate operating cycles and the denitrification process within an SBR.

KEYWORDS: convection-diffusion-reaction PDE, degenerate parabolic PDE, moving boundary, numerical scheme, sedimentation, sequencing batch reactor

2000 MATH SUBJECT CLASSIFICATION: 35K65, 35Q35, 65M06, 76V05

1. INTRODUCTION

1.1. Scope. We present a one-dimensional model of reactive sedimentation in a tank (with a possibly varying cross-sectional area). At the bottom, the tank has a controlled outlet. At the surface of the mixture, a floating device allows for controlled fill or extraction of mixture; see Figure 1 (a). The settling particles consist of several components, which react with other dissolved material components. We also present a numerical method for the simulation of such a general process, which can handle any feed or extraction condition where the volume of mixture in the tank may vary between zero (surface at the bottom) and maximal (surface at the top). The specific application we have in mind

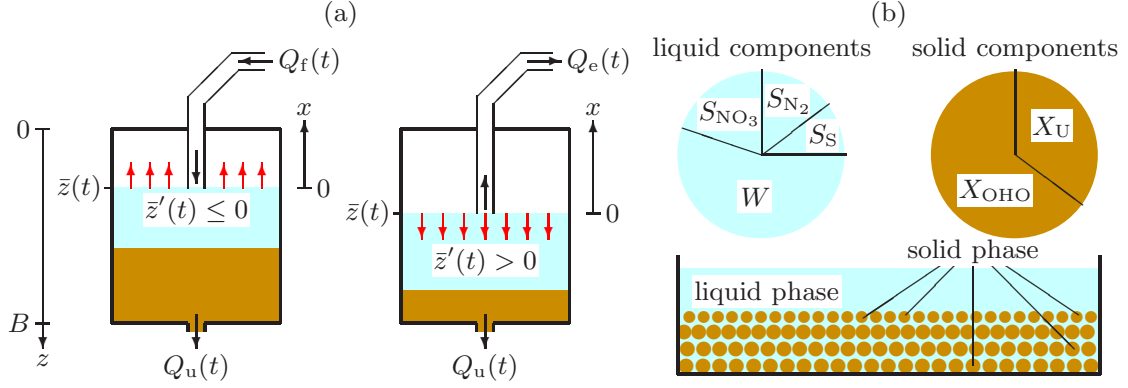


Figure 1. (a) Left: Fill at the volume rate $Q_f(t) > 0$ greater than the underflow rate $Q_u(t) \geq 0$ resulting in a rise of the mixture surface location $z = \bar{z}(t)$. Right: Draw (extraction) of mixture from the surface at the rate $Q_e(t) > 0$ implies a descending surface. (b) The two phases and their components for the examples of denitrification in Section 5.

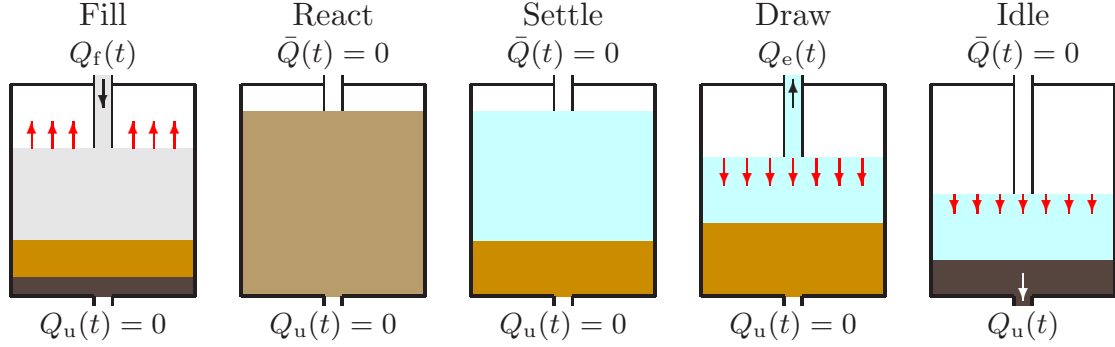


Figure 2. The five stages of a cycle of an SBR. The tank is first filled with wastewater at the volumetric flow $Q_f(t) > 0$ and concentrations $\mathbf{C}_f(t)$ and $\mathbf{S}_f(t)$. During the react stage, biological reactions take place under complete mixing by an impeller or by aeration. Then batch sedimentation with reactions occurs and liquid is extracted during the draw stage. During the idle stage, some of the bottom sludge can be withdrawn and then the fill stage starts again.

is a *sequencing batch reactor* (SBR), which is commonly used for wastewater treatment, where batch operations of reactions and sedimentation are applied in sequence in time, with fill and draw (extraction) operations between or during these stages; see Figure 2. In an SBR, the particles are biomass (bacteria; activated sludge) and the dissolved materials are substrates (nitrogen, phosphorus, etc.) to be removed. Other applications arise, for example, in mineral processing where mineral powders are flocculated by adding liquid flocculant dissolved in water.

To introduce the governing model, we let $A = A(z)$ denote the cross-sectional area of the tank that may depend on depth z , where $z = 0$ at the top of the tank and $z = B$ at its bottom. The characteristic function γ equals one inside the mixture and zero otherwise, i.e., $\gamma(z, t) = \chi_{\{\bar{z}(t) < z < B\}}$, where χ_I is the indicator function which equals one if and only if I is true, and $z = \bar{z}(t)$ is the surface location. The unknowns are the vectors $\mathbf{C} = \mathbf{C}(z, t) = (C^{(1)}, \dots, C^{(k_C)})^T$ of solid concentrations and of $\mathbf{S} = \mathbf{S}(z, t) = (S^{(1)}, \dots, S^{(k_S)})^T$ concentrations of soluble components. These vectors make up the components of the solid and liquid phase, respectively. With $X = X(z, t) =$

$C^{(1)}(z, t) + \dots + C^{(k_C)}(z, t)$, the tank can be modeled as the following system of convection-diffusion-reaction equations, where $t > 0$ is time:

$$\begin{aligned} A(z)\partial_t \mathbf{C} + \partial_z(A(z)\mathcal{F}_C(X, z, t)\mathbf{C}) - \partial_z(A(z)\gamma(z, t)(\partial_z D(X))\mathbf{C}) \\ = \delta(z - \bar{z}(t))Q_f(t)\mathbf{C}_f(t) + \gamma(z, t)A(z)\mathbf{R}_C(\mathbf{C}, \mathbf{S}), \\ A(z)\partial_t \mathbf{S} + \partial_z(A(z)\mathcal{F}_S(X, z, t)\mathbf{S}) \\ = \delta(z - \bar{z}(t))Q_f(t)\mathbf{C}_f(t) + \gamma(z, t)A(z)\mathbf{R}_S(\mathbf{C}, \mathbf{S}). \end{aligned} \quad (1)$$

This system is coupled to a model of the effluent pipe consisting of convective transport equations on a half line $x \geq 0$, where $x = 0$ is attached to the moving boundary $z = \bar{z}(t)$ (cf. Figure 1 (a)). The coupling conditions between the systems are mass-preserving algebraic equations with fluxes on the z - and x -axes. The scalar functions \mathcal{F}_C and \mathcal{F}_S in (1) depend nonlinearly on X and represent portions of the solid- and liquid-phase velocity, respectively. The scalar function D models sediment compressibility. The terms with the delta function $\delta(z - \bar{z}(t))$ model the operation of the device floating on the surface for either feed or extraction of mixture. The last term of each PDE contains the reaction rates (local increase of mass per unit time and volume) \mathbf{R}_C and \mathbf{R}_S . The full PDE model is specified in Section 2. During the react stage of an SBR (see Figure 2), full mixing occurs and the system of PDEs (1) reduces to a system of ordinary differential equations (ODEs).

The main difficulties for the analysis of the model arise partly from the presence of a moving boundary where both a source is located and a half-line model attached, and partly from strong type degeneracy; the function D is zero for X -values on an interval of positive length. The main purpose of this work is to introduce a numerical scheme that handles these difficulties and produces approximate solutions that satisfy certain bounds under a convenient Courant-Friedrichs-Lewy (CFL) condition. In particular, the scheme is positivity preserving.

1.2. Related work. The SBR technology has been used for hundred years and been a topic for much research [35]. Its usage for wastewater treatment can be found in many handbooks (e.g., [12, 16, 30]). Furthermore, it is also employed for recovery of selenium [36], radioactively labelled pharmaceuticals [34], nitrogen removal processes [31], pharmaceutically active compounds [38], synthetic chemical components [21], swine manure slurry [28], applications in the petrochemical industry [10] and saline wastewater treatment [2] among others.

Most treatments in the literature on mathematical models related to SBRs focus on ODEs modeling the reactions by established activated sludge models [17, 20, 24, 29]. Optimization and control problems [18, 25, 32, 33, 37] and statistical methods [26, 27]. Less consideration has been laid on the sedimentation in an SBR during which reactions occur. Models of reactive settling in continuously operated secondary settling tanks (SSTs) based on PDEs are presented in [5, 6, 7] (see also references cited in these works). It is worth pointing out that the SBR model differs from an SST model. In an SBR, $Q_u(t)$, $Q_f(t)$ and $Q_e(t)$ are given independent control functions giving rise to a moving surface, whereas in an SST, only two of these are known and the third, often $Q_e(t)$, is defined by the other two and possibly by volume-changing reactions in the tank [8].

The moving-boundary problem (1) with a connected half-axis with transport equations has nonlinear mass-preserving coupling conditions, which do not define the coupling concentrations uniquely. Such a problem of nonuniqueness arises already for a scalar conservation law with discontinuous flux, which has been investigated widely [1, 3, 13, 19, 22, 23]; in particular, in the context of continuous sedimentation [4, 9, 11, 14, 15] where a monotone numerical scheme approximates the correct solutions [9].

1.3. Outline of the paper. In Section 2, we derive the model. Section 3 contains the numerical scheme based in the line of [5] modified to handle the moving boundary. The fully discrete scheme is presented in Section 3.4 and the CFL condition and invariant-region property are shown in Section 3.5. Section 4 contains a derivation of the ODE model for full mixing. In Section 5, we show two numerical examples of SBR operation with a constant cross-sectional area (cylindrical vessel) and a variable. Some conclusions are collected in Section 6.

2. DERIVATION OF THE MODEL OF REACTIVE SETTLING

2.1. Preliminaries. The solid phase consists of flocculated particles of k_C types with concentrations $C^{(1)}, \dots, C^{(k_C)}$. The components of the liquid phase are water of concentration W and k_S dissolved substrates of concentrations $S^{(1)}, \dots, S^{(k_S)}$ (cf. Figure 1 (b)). The total concentrations of solids X and liquid L are

$$X := C^{(1)} + \dots + C^{(k_C)}, \quad L := W + S^{(1)} + \dots + S^{(k_S)}. \quad (2)$$

All these concentrations depend on z and t , and our notation is the same as in [5].

For computational purposes, we define a maximum concentration \hat{X} of solids and assume that the density of all solids is the same, namely $\rho_X > \hat{X}$. Similarly, we assume that the liquid phase has the density $\rho_L < \rho_X$, typically the density of water.

The reaction terms for all components are collected in the vectors $\mathbf{R}_C(\mathbf{C}, \mathbf{S})$ and $\mathbf{R}_S(\mathbf{C}, \mathbf{S})$, which model the increase of solid and soluble components, respectively, and set $\tilde{\mathbf{R}}_C(\mathbf{C}, \mathbf{S}) := R_C^{(1)}(\mathbf{C}, \mathbf{S}) + \dots + R_C^{(k_S)}(\mathbf{C}, \mathbf{S})$ (analogously for $\tilde{\mathbf{R}}_S(\mathbf{C}, \mathbf{S})$). The water concentration W is not active in any reaction. We assume that without bacteria there is no growth; $\mathbf{R}_C(\mathbf{0}, \mathbf{S}) = \mathbf{0}$, and when there is no substrate, the bacteria cannot consume any such, however, substrate concentrations may increase due to decay of bacteria. Hence, we assume $\mathbf{R}_S(\mathbf{C}, \mathbf{0}) \geq \mathbf{0}$, but $\mathbf{R}_S(\mathbf{0}, \mathbf{0}) = \mathbf{0}$, where vector inequalities are understood component-wise. If one sort of bacteria is not present; no more such can vanish, i.e.,

$$R_C^{(k)}(\mathbf{C}, \mathbf{S})|_{C^{(k)}=0} \geq 0 \quad \text{for } k = 1, \dots, k_C. \quad (3)$$

We let v_X and v_L denote the velocities of the solid and liquid phases, respectively. It is assumed that the relative velocity $v_X - v_L =: v_{\text{rel}} = v_{\text{rel}}(X, \partial_z X, z)$ is given by a constitutive function of X and its spatial derivative $\partial_z X$, modeling hindered and compressive settling; see Section 2.3. The following technical assumptions are made to establish an invariant-region property for the numerical solution:

$$\mathbf{R}_C(\mathbf{C}, \mathbf{S})|_{X=\hat{X}} = \mathbf{0}, \quad v_{\text{rel}}(\hat{X}, \partial_z X, z) = 0. \quad (4)$$

These conditions mean that when the maximum concentration is reached ($X = \hat{X}$), biomass cannot grow any more and its relative velocity to the liquid phase is zero.

It is assumed that in the inlet and outlet pipes no reactions take place and all components have the same velocity. At the bottom, $z = B$, one can withdraw mixture at a given volume rate $Q_u(t) \geq 0$. The underflow region $z > B$ is for simplicity modelled by setting $A(z) := A(B)$, since we are only interested in the underflow concentration $\mathbf{C}_u(t)$, which is an outcome of the model (analogously for $\mathbf{S}_u(t)$).

At the surface of the mixture, $z = \bar{z}(t)$, we model a floating device connected to a pipe through which one can feed the tank with a given volume rate $Q_f(t)$ and given feed concentrations $\mathbf{C}_f(t)$ and $\mathbf{S}_f(t)$; see Figure 1. This gives rise to a source term in the model equation with the fluxes $Q_f(t)\mathbf{C}_f(t)$ and $Q_f(t)\mathbf{S}_f(t)$. Alternatively, this floating device allows to extract mixture at a given volume rate $Q_e(t) > 0$ through the same pipe; hence, one cannot fill and extract simultaneously. If $[0, T]$ denotes the total time interval of modeling, we assume that $T := T_e \cup T_f$, where

$$T_e := \{t \in \mathbb{R}_+ : Q_e(t) > 0, Q_f(t) = 0\}, \quad T_f := \{t \in \mathbb{R}_+ : Q_e(t) = 0, Q_f(t) \geq 0\}.$$

When $t \in T_e$, we model the extraction flow in the effluent pipe by a moving coordinate system; a half line $x \geq 0$, where $x = 0$ is attached to $z = \bar{z}(t)$. Along this half line, we denote the solids concentration by $\tilde{\mathbf{C}} = \tilde{\mathbf{C}}(x, t)$. The effluent concentration $\mathbf{C}_e(t) := \tilde{\mathbf{C}}(0^+, t)\chi_{\{t \in T_e\}}$ is also a model outcome (analogously for $\mathbf{S}_e(t)$).

It is convenient to define the volume fractions

$$\phi := X/\rho_X, \quad \phi_L := L/\rho_L, \quad \phi_M := \phi + \phi_L, \quad (5)$$

where the volume fraction of the mixture satisfies $\phi_M = \chi_{\{z > \bar{z}(t)\}}$. Below the surface, $\phi + \phi_L = 1$, or equivalently, $L = \rho_L(1 - X/\rho_X)$. The same holds for the feed concentrations. For known \mathbf{C} and \mathbf{S} , (2) implies the water concentration

$$W = \rho_L(1 - X/\rho_X) - (S^{(1)} + \dots + S^{(ks)}). \quad (6)$$

This concentration is not part of any reaction and can be computed afterwards.

The volume of the mixture is defined by

$$\bar{V}(t) := V(\bar{z}(t)), \quad \text{where} \quad V(z) := \int_z^B A(\xi) d\xi \quad \text{for } 0 \leq z \leq B. \quad (7)$$

The function V is invertible since $V'(z) = -A(z) < 0$; in particular,

$$\bar{V}'(t) = V'(\bar{z}(t))\bar{z}'(t) = -A(\bar{z}(t))\bar{z}'(t). \quad (8)$$

2.2. Balance laws. The balance laws for all components in local form imply

$$\partial_t(A(z)\mathbf{C}) + \partial_z(A(z)v_X\mathbf{C}) = \delta(z - \bar{z}(t))Q_f\mathbf{C}_f + \gamma(z, t)A(z)\mathbf{R}_\mathbf{C}, \quad z \in \mathbb{R}, \quad (9a)$$

$$\partial_t(A(z)\mathbf{S}) + \partial_z(A(z)v_L\mathbf{S}) = \delta(z - \bar{z}(t))Q_f\mathbf{S}_f + \gamma(z, t)A(z)\mathbf{R}_\mathbf{S}, \quad z \in \mathbb{R}. \quad (9b)$$

This system along with $v_{\text{rel}} = v_X - v_L$ and (5) are $k_\mathbf{C} + k_\mathbf{S} + 2$ equations for the same number of scalar unknowns, i.e., the components of \mathbf{C} and \mathbf{S} , plus v_X and v_L . It is coupled to the following model of the effluent pipe:

$$\partial_t\tilde{\mathbf{C}} + Q_e\partial_x\tilde{\mathbf{C}} = \mathbf{0}, \quad x > 0, \quad (10a)$$

$$\partial_t\tilde{\mathbf{S}} + Q_e\partial_x\tilde{\mathbf{S}} = \mathbf{0}, \quad x > 0, \quad (10b)$$

$$-Q_e(t)\tilde{\mathbf{C}}(0^+, t) = A(\bar{z}(t)^+)(v_X|_{z=\bar{z}(t)^+} - \bar{z}'(t))\mathbf{C}(\bar{z}(t)^+, t), \quad (10c)$$

$$-Q_e(t)\tilde{\mathbf{S}}(0^+, t) = A(\bar{z}(t)^+)(v_L|_{z=\bar{z}(t)^+} - \bar{z}'(t))\mathbf{S}(\bar{z}(t)^+, t). \quad (10d)$$

The coupling equations (10c) and (10d) preserve mass at the surface during extraction periods. The purpose of (10) is to define the concentrations during periods of extraction when $Q_e(t) > 0$. The outlet concentrations are given by, for $t > 0$,

$$\mathbf{C}_u(t) := \mathbf{C}(B^+, t), \quad \mathbf{S}_u(t) := \mathbf{S}(B^+, t), \quad (11)$$

$$\mathbf{C}_e(t) := \tilde{\mathbf{C}}(0^+, t)\chi_{\{t \in T_e\}}, \quad \mathbf{S}_e(t) := \tilde{\mathbf{S}}(0^+, t)\chi_{\{t \in T_e\}}. \quad (12)$$

The transport PDEs (10a) and (10b) are easily solved once the boundary data (12) are known, which in turn have to satisfy (10c) and (10d). The right-hand sides of the latter equations are however nonlinear functions of $\mathbf{C}(\bar{z}(t)^+, t)$ (via v_X and v_L) and to obtain unique boundary concentrations on either side of a spatial discontinuity, an additional entropy condition is needed. Our experience is, however, that correct concentrations can be obtained by a conservative and monotone numerical method [9].

The volume-average bulk velocity is defined by $q(z, t) := (\phi v_X + \phi_L v_L)\chi_{\{z > \bar{z}(t)\}}$. Since $\phi_M = 0$ for $z < \bar{z}(t)$, we have $\phi = \phi_L = 0$ there. Summing all the equations of (9a) and (9b), respectively, and using (2) and (5), we get the scalar PDEs

$$\begin{aligned} \partial_t(A(z)\rho_X\phi) + \partial_z(A(z)\rho_X\phi v_X) &= \delta(z - \bar{z}(t))\rho_X\phi_f Q_f + \gamma(z, t)A(z)\tilde{R}_\mathbf{C}, \\ \partial_t(A(z)\rho_L\phi_L) + \partial_z(A(z)\rho_L\phi_L v_L) &= \delta(z - \bar{z}(t))\rho_L\phi_{L,f} Q_f + \gamma(z, t)A(z)\tilde{R}_\mathbf{S}. \end{aligned}$$

Dividing away the constant densities and adding the results, we get

$$\partial_t(A(z)\phi_M) + \partial_z(A(z)q) = \delta(z - \bar{z}(t))\phi_{M,f}Q_f + \gamma(z, t)A(z)\mathcal{R}, \quad (13)$$

where $\mathcal{R} := \tilde{R}_C/\rho_X + \tilde{R}_S/\rho_L$, and $\phi_{M,f} = 1$ by definition. The first term of (13) is

$$\partial_t(A(z)\phi_M) = A(z)\partial_t\chi_{\{z > \bar{z}(t)\}} = -A(z)\delta(z - \bar{z}(t))\bar{z}'(t).$$

The same procedure for the algebraic equations (10c) and (10d) ($t \in I_e$) yields

$$-Q_e(t) = A(\bar{z}(t)^+)(q(\bar{z}(t)^+, t) - \bar{z}'(t)). \quad (14)$$

Integrating (13) (with or without the source term) from $z \in (\bar{z}(t)^+, B)$ to B , we get

$$A(B)q(B, t) - A(z)q(z, t) = \int_z^B A(\xi)\mathcal{R}(C(\xi, t), S(\xi, t)) d\xi =: Q_{\text{reac}}(z, t; C, S),$$

where $A(B)q(B, t) = Q_u(t)$. Hence, inside the mixture, i.e., in the interval $(\bar{z}(t), B)$, the volume-average velocity q is given by $A(z)q(z, t) = Q_u(t) - Q_{\text{reac}}(z, t; C, S)$. In view of this equation and $q = (\phi v_X + \phi_L v_L)\chi_{\{z > \bar{z}(t)\}}$, we integrate (13) from $z = \bar{z}(t) - h$ to $\bar{z}(t) + h$ and let $0 < h \rightarrow 0$ to get

$$-A(\bar{z}(t))\bar{z}'(t) + Q_u(t) - Q_{\text{reac}}(z, t; C, S)|_{z=\bar{z}(t)} = Q_f(t), \quad (15)$$

where the first term can be written $\bar{V}'(t)$; see (8). For $t \in T_e$, (14) implies

$$-Q_e(t) = Q_u(t) - Q_{\text{reac}}(z, t; C, S)|_{z=\bar{z}(t)} + V'(t). \quad (16)$$

The term Q_{reac} seems to be negligible [7] in the application to wastewater treatment. We set $Q_{\text{reac}} := 0$ from now on, which makes it possible to prove an invariant-region property of the numerical solutions; see Section 3.5. Consequently, we define

$$q(z, t) := (Q_u(t)/A(z))\chi_{\{z > \bar{z}(t)\}}. \quad (17)$$

Then (15) and (16) can be written (with $Q_{\text{reac}} = 0$) as

$$\bar{V}'(t) = \bar{Q}(t) - Q_u(t), \quad \text{where} \quad \bar{Q}(t) = \begin{cases} -Q_e(t) < 0 & \text{if } t \in T_e, \\ Q_f(t) \geq 0 & \text{if } t \in T_f. \end{cases} \quad (18)$$

Solving this ODE and utilizing (7), we obtain

$$\bar{z}(t) = V^{-1} \left(\bar{V}(0) + \int_0^t (\bar{Q}(s) - Q_u(s)) ds \right). \quad (19)$$

Alternatively, $\bar{z}(t)$ can be obtained from (see (8))

$$\bar{z}'(t) = \frac{Q_u(t) - \bar{Q}(t)}{A(\bar{z}(t))}. \quad (20)$$

2.3. Constitutive functions for hindered and compressive settling. The surface location $z = \bar{z}(t)$ is now specified, so we may focus on the mixture in $z > \bar{z}(t)$. For the given functions q and the relative velocity v_{rel} , we set $v := (1 - \phi)v_{\text{rel}}$, and obtain from $v_{\text{rel}} = v_X - v_L$ and $q = (\phi v_X + \phi_L v_L)\chi_{\{z > \bar{z}(t)\}}$ the phase velocities

$$v_X = q + (1 - \phi)v_{\text{rel}} = q + v \quad \text{and} \quad v_L = q - \phi v_{\text{rel}} = q - \frac{\phi}{1 - \phi}v \quad (21)$$

of the solid and fluid, respectively. We assume that the relative velocity $v_{\text{rel}} = v/(1 - \phi)$, where $\phi = X/\rho_X$, and where v is the commonly used expression [8, 9]

$$v(X, \partial_z X, z, t) := \gamma(z, t)v_{\text{hs}}(X) \left(1 - \frac{\rho_X \sigma'_e(X)}{X g \Delta \rho} \partial_z X \right) = \gamma(z, t)(v_{\text{hs}}(X) - \partial_z D(X)), \quad (22)$$

where

$$D(X) := \int_{X_c}^X d(s) ds, \quad d(X) := v_{\text{hs}}(X) \frac{\rho_X \sigma'_e(X)}{g X \Delta \rho},$$

Here, $\Delta\rho := \rho_X - \rho_L$, g is the acceleration of gravity, $v_{\text{hs}} = v_{\text{hs}}(X)$ is the hindered-settling velocity, which is assumed to be decreasing and satisfy $v_{\text{hs}}(\hat{X}) = 0$, $\sigma_e = \sigma_e(X)$ the effective solids stress, which satisfies $\sigma'_e(X) = 0$ for $X \leq X_c$ and $\sigma'_e(X) > 0$ for $X > X_c$, where X_c is a critical concentration above which the particles touch each other and form a network that can bear a certain stress. Note that $d(X) = 0$ for $X \leq X_c$, which causes the strongly degenerate-type behavior.

2.4. Model equations in final form. With q defined by (17), we define and use (21) and (22) to write the velocities

$$\begin{aligned}\mathcal{F}_C(X, z, t) &:= q(z, t) + \gamma(z, t)v_{\text{hs}}(X), \\ \mathcal{F}_S(X, z, t) &:= \frac{\rho_X q(z, t) - (q(z, t) + \gamma(z, t)v_{\text{hs}}(X))X}{\rho_X - X},\end{aligned}\tag{23}$$

and then express the total mass fluxes of the balance laws (9) in light of (21):

$$\begin{aligned}\Phi_C &:= \Phi_C(C, X, \partial_z X, z, t) := A(z)v_X(X, \partial_z X, z, t)C \\ &= A(z)(\mathcal{F}_C(X, z, t) - \gamma(z, t)\partial_z D(X)), \\ \Phi_S &:= \Phi_S(S, X, \partial_z X, z, t) := A(z)\frac{\rho_X q - v_X X}{\rho_X - X}S = A(z)\mathcal{F}_S(X, z, t),\end{aligned}$$

Then we define and rewrite the right-hand side of (10c) with (20), (21) and (22):

$$\begin{aligned}\Phi_{C,e}(t) &:= A(\bar{z}(t))(v_X(\bar{z}(t)^+, t) - \bar{z}'(t))C(\bar{z}(t)^+, t) \\ &= \left(A(q + v_{\text{hs}}(X) - \partial_z D(X)) - Q_u - Q_e\right)C\Big|_{z=\bar{z}(t)^+} \\ &= \left(A(v_{\text{hs}}(X) - \partial_z D(X)) - Q_e\right)C\Big|_{z=\bar{z}(t)^+}.\end{aligned}\tag{24}$$

Analogously, we define $\Phi_{S,e}$ corresponding to (10d):

$$\begin{aligned}\Phi_{S,e}(t) &:= A(\bar{z}(t))(v_L(\bar{z}(t)^+, t) - \bar{z}'(t))S(\bar{z}(t)^+, t) \\ &= \left(A\left(q - \frac{X(v_{\text{hs}}(X) - \partial_z D(X))}{\rho_X - X}\right) - (Q_u + Q_e)\right)S\Big|_{z=\bar{z}(t)^+} \\ &= -\left(A\frac{X(v_{\text{hs}}(X) - \partial_z D(X))}{\rho_X - X} + Q_e\right)S\Big|_{z=\bar{z}(t)^+}.\end{aligned}\tag{25}$$

The final model can now be described as follows. Given the in- and outgoing volumetric flows, one computes the surface level by (19) or (20). The concentrations C and S are given by the system (9), which can be written as

$$A(z)\partial_t C + \partial_z \Phi_C = \delta(z - \bar{z}(t))Q_f C_f + \gamma(z, t)A(z)R_C,\tag{26a}$$

$$A(z)\partial_t S + \partial_z \Phi_S = \delta(z - \bar{z}(t))Q_f S_f + \gamma(z, t)A(z)R_S,\tag{26b}$$

or as (1). The water concentration W can always be calculated from (6). Note that W is not present in (1), (23). The effluent and underflow concentrations are given by (11) and (12), respectively. No initial data are needed for the outlet concentrations, but for the following:

$$C^0 = (C^{(1),0}, C^{(2),0}, \dots, C^{(k_C),0})^T, \quad S^0 = (S^{(1),0}, S^{(2),0}, \dots, S^{(k_S),0})^T.$$

3. NUMERICAL SCHEME

3.1. Spatial discretization and numerical fluxes. We divide the tank into N computational cells each having depth $h = B/N$. Assume that the midpoint of cell j has the coordinate z_j , hence, the cell is the interval $[z_{j-1/2}, z_{j+1/2}]$. The top cell 1 is thus $[z_{1/2}, z_{3/2}] = [0, h]$, and the bottom location is $z = z_{N+1/2} = B$. To obtain the underflow

concentrations, we add one cell below $z = B$. To obtain the extraction concentrations, we add one cell on the x -coordinate system; $[0, \Delta x]$. To approximate the cell volumes, we define the average cross-sectional areas

$$A_{j-1/2} := \frac{1}{h} \int_{z_{j-1}}^{z_j} A(\xi) d\xi \quad \text{and} \quad A_j := \frac{1}{h} \int_{z_{j-1/2}}^{z_{j+1/2}} A(\xi) d\xi.$$

The unknowns are approximated by functions that are piecewise constant in each cell j , i.e. $C^{(k)}(z, t) \approx C_j^{(k)}(t)$, $z \in [z_{j-1/2}, z_{j+1/2}]$, which are collected in the vector $\mathbf{C}_j(t)$. We define $\bar{j}(t) := \lceil \bar{z}(t)/h \rceil$, which is the smallest integer larger than or equal to $\bar{z}(t)/h$. Then the surface $z = \bar{z}(t)$ is located in the surface cell $\bar{j}(t)$.

We let $\gamma_{j+1/2}(t) := \gamma(z_{j+1/2}, t)$ and define the approximate volume-average velocity $q_{j+1/2}(t) := q(z_{j+1/2}, t)$ in accordance with (17) with $Q_{\text{reac}} \equiv 0$ via

$$A_{j+1/2} q_{j+1/2}(t) := Q_u(t) \chi_{\{j+1/2 > \bar{j}(t)\}}.$$

Using the notation $a^- := \min\{a, 0\}$ and $a^+ := \max\{a, 0\}$, we define

$$\begin{aligned} J_{j+1/2}^{\mathbf{C}} &= J_{j+1/2}^{\mathbf{C}}(X_j, X_{j+1}) := (D(X_{j+1}) - D(X_j))/h, \\ v_{j+1/2}^X &= v_{j+1/2}^X(X_j, X_{j+1}, t) := q_{j+1/2} + \gamma_{j+1/2}(v_{\text{hs}}(X_{j+1}) - J_{j+1/2}^{\mathbf{C}}), \\ F_{j+1/2}^X &= F_{j+1/2}^X(X_j, X_{j+1}, t) := (v_X X)_{j+1/2} := v_{j+1/2}^{X,-} X_{j+1} + v_{j+1/2}^{X,+} X_j, \\ \Phi_{j+1/2}^{\mathbf{C}} &:= A_{j+1/2} (v_{j+1/2}^{X,-} \mathbf{C}_{j+1} + v_{j+1/2}^{X,+} \mathbf{C}_j), \\ \Phi_{j+1/2}^{\mathbf{S}} &:= A_{j+1/2} \left(\frac{(\rho_X q_{j+1/2} - F_{j+1/2}^X)^-}{\rho_X - X_{j+1}} \mathbf{S}_{j+1} + \frac{(\rho_X q_{j+1/2} - F_{j+1/2}^X)^+}{\rho_X - X_j} \mathbf{S}_j \right). \end{aligned} \quad (27)$$

In particular, we have $\Phi_{j+1/2}^{\mathbf{C}} = \Phi_{j+1/2}^{\mathbf{S}} = \mathbf{0}$ for $j < \bar{j}(t)$. We denote by $[\Delta \Phi]_j := \Phi_{j+1/2} - \Phi_{j-1/2}$ the flux difference associated with cell j . For the single cell on the x -axis, the fluxes at $x = \Delta x$ are $Q_e(t) \mathbf{C}_e(t)$ and $Q_e(t) \mathbf{S}_e(t)$; see (10a) and (10b).

3.2. Time discretization and surface fluxes. We let T denote the total simulation time, t_n , $n = 0, 1, \dots, N_T$, the discrete time points and $\tau := T/N_T$ the time step that should satisfy a certain CFL condition; see below. The value of a variable at time t_n is denoted by an upper index, e.g., \mathbf{C}_j^n and it is thus assumed to be constant in time during $t_n \leq t < t_{n+1}$. The discrete surface index is defined by $\bar{j}^n := \bar{j}(t_n)$ and we let $\bar{z}^n := \bar{z}(t_n)$. For the volumetric flows, we define the averages

$$Q_{\text{f}}^n := \frac{1}{\tau} \int_{t_n}^{t_{n+1}} Q_{\text{f}}(t) dt$$

and assume for simplicity that any of the volumetric flows changes sign at most at the discrete time points t_n . This implies that $\bar{z}(t)$ is monotone on every interval $[t_n, t_{n+1}]$. To ensure that the surface does not travel more than one cell width h during τ , the CFL condition has to imply (cf. (20))

$$\tau \max_{0 \leq t \leq T} |\bar{z}'(t)| \leq \tau \max_{\substack{0 \leq t \leq T, \\ 0 \leq z \leq B}} \left\{ \frac{|Q_u(t) - Q_f(t)|}{A(z)}, \frac{|Q_u(t) + Q_e(t)|}{A(z)} \right\} \leq h. \quad (28)$$

To show that the cell concentrations $\mathbf{C}_{\bar{j}^n}^n$ do not exceed the maximal one \hat{X} , we also introduce the concentration $\bar{\mathbf{C}}_{\bar{j}^n}^n$ obtained when all the mass in the surface cell \bar{j}^n is located below the surface within the cell; cf. Figure 3(a). The mass in the cell is

$$\bar{\mathbf{C}}_{\bar{j}^n}^n A_j \alpha^n h = \mathbf{C}_{\bar{j}^n}^n A_j h, \quad \text{where} \quad \alpha^n h := z_{\bar{j}^n+1/2} - \bar{z}^n. \quad (29)$$

We set $\bar{X}_j^n := \bar{C}_j^{(1),n} + \dots + \bar{C}_j^{(k_C),n}$. Integrating (18) from t_n to t_{n+1} , one obtains

$$V(\bar{z}(t_{n+1})) - V(\bar{z}(t_n)) = (\bar{Q}^n - Q_u^n) \tau. \quad (30)$$

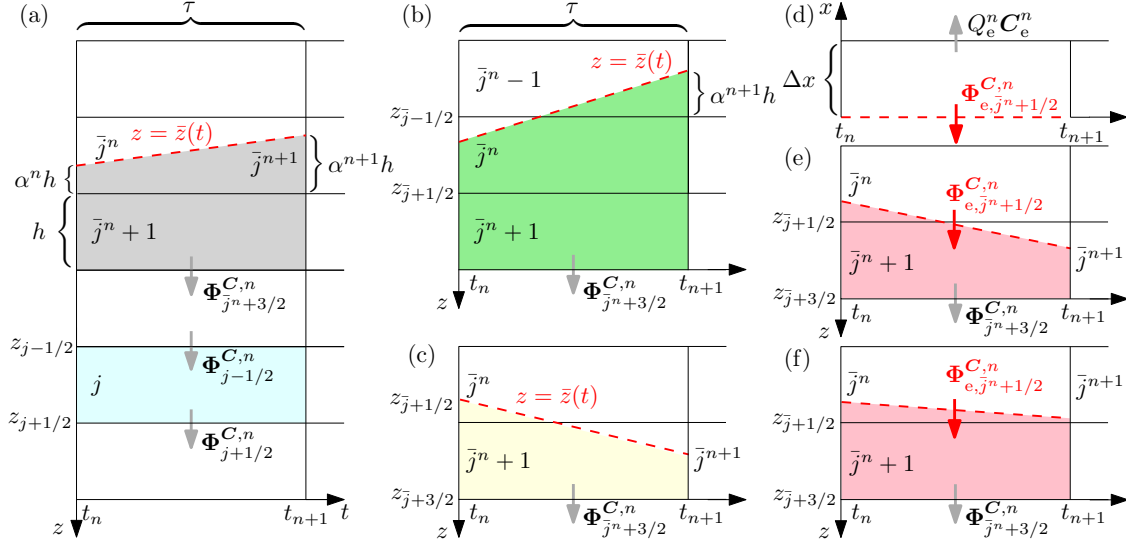


Figure 3. Fluxes over cell boundaries shown by grey arrows and the flux at the surface with red arrows. The surface level $z = \bar{z}(t)$ is drawn with a red dashed line. Plot (d) shows the extraction pipe cell where the origin of the x -axis located on the red dashed surface $z = \bar{z}(t)$ in plots (e) and (f).

If the surface stays within one cell between t_n and t_{n+1} ; then (30) is equivalent to

$$A_j(\alpha^{n+1} - \alpha^n)h = (\bar{Q}^n - Q_u^n)\tau \quad (31)$$

(cf. Figure 3(a) and (f)). During extraction, the surface cannot rise and is thus located somewhere in cells \bar{j}^n and $\bar{j}^n + 1$ (cf. Figure 3(c), (e) and (f)). In light of (24) and (25), we approximate the fluxes, which have to be nonpositive, just below the surface in the following way:

$$v_{e,\bar{j}^n+1/2}^{X,n} := v_{hs}(X_{\bar{j}^n+1}^n) - D(X_{\bar{j}^n+1}^n)/h - Q_e^n/A_{\bar{j}^n+1/2}, \quad (32)$$

$$\Phi_{e,\bar{j}^n+1/2}^{C,n} := A_{\bar{j}^n+1/2} v_{e,\bar{j}^n+1/2}^{X,n,-} C_{\bar{j}^n+1}^n, \quad (33)$$

$$\Phi_{e,\bar{j}^n+1/2}^{S,n} := \left(-\frac{A_{\bar{j}^n+1/2} X_{\bar{j}^n+1}^n}{\rho_X - X_{\bar{j}^n+1}^n} (v_{hs}(X_{\bar{j}^n+1}^n) - D(X_{\bar{j}^n+1}^n)/h) - Q_e^n \right)^- S_{\bar{j}^n+1}^n. \quad (34)$$

3.3. Derivation of update formulas. We here derive the update formulas for C_j^n . Analogous formulas hold for S_j^n when replacing C by S ; however, with different definitions of velocities and fluxes. First come cells that lie below the surface $z = \bar{z}(t)$ at t_n and t_{n+1} . Special treatment is needed for the cells near the surface. All cells strictly above the surface have zero concentrations. Let $\kappa := \tau/h$.

Cells away from the surface. Using the integrated form of the balance law on a rectangle $[z_{j-1/2}, z_{j+1/2}] \times [t_n, t_{n+1}]$ strictly below the surface; see the blue rectangle in Figure 3(a), we get the update formula (mass per h)

$$A_j C_j^{n+1} = A_j C_j^n + \kappa(-[\Delta \Phi^C]_j^n + A_j R_{C,j}^n),$$

and the analogous one for S_j^n . For cell $N+1$, we get in the similar way the update formula for the underflow concentration; see Section 3.4.

Cells near the surface during fill ($t \in T_f$). To obtain a monotone scheme with an invariant-region property, we see how the mass in the surface cell and the one below evolves; see the trapezoids in Figure 3. The mass per h at t_n is (we use (29))

$$m_{\bar{j}^n}^{C,n} = A_j \alpha^n \bar{C}_{\bar{j}^n}^n + A_{\bar{j}^n+1} C_{\bar{j}^n+1}^n = A_{\bar{j}^n} C_{\bar{j}^n}^n + A_{\bar{j}^n+1} C_{\bar{j}^n+1}^n. \quad (35)$$

During τ , the feed source along the moving surface is $Q_f^n \mathbf{C}_f^n$, whereas the outflux is $\Phi_{\bar{j}^n+3/2}^{C,n}$. Thus, by the balance law on any trapezoid the mass (per h) at t_{n+1} is

$$\mathbf{m}_{\bar{j}^n}^{C,n+1} = \mathbf{m}_{\bar{j}^n}^{C,n} + \kappa \Psi_{\bar{j}^n}^{C,n} \quad (36)$$

where the in- and outflux and source terms are

$$\Psi_{\bar{j}^n}^{C,n} := Q_f^n \mathbf{C}_f^n - \Phi_{\bar{j}^n+3/2}^{C,n} + h(A_{\bar{j}^n} \mathbf{R}_{\mathbf{C},\bar{j}^n}^n + A_{\bar{j}^n+1} \mathbf{R}_{\mathbf{C},\bar{j}^n+1}^n). \quad (37)$$

Fill case $\bar{j}^n = \bar{j}^{n+1}$, Figure 3 (a): When the surface does not cross any cell boundary during τ , the mass (36) is distributed among the two cells with respect to their volumes (below the surface):

$$\begin{aligned} A_{\bar{j}^n} \mathbf{C}_{\bar{j}^n}^{n+1} &= \frac{\alpha^{n+1} A_{\bar{j}^n}}{\alpha^{n+1} A_{\bar{j}^n} + A_{\bar{j}^n+1}} \mathbf{m}_{\bar{j}^n}^{C,n+1}, \\ A_{\bar{j}^n+1} \mathbf{C}_{\bar{j}^n+1}^{n+1} &= \frac{A_{\bar{j}^n+1}}{\alpha^{n+1} A_{\bar{j}^n} + A_{\bar{j}^n+1}} \mathbf{m}_{\bar{j}^n}^{C,n+1}. \end{aligned} \quad (38)$$

Fill case $\bar{j}^n = \bar{j}^{n+1} + 1$, Figure 3 (b): After the balance law is used on the green trapezoid, the final mass (per h) is distributed among three cells:

$$\begin{aligned} A_{\bar{j}^n-1} \mathbf{C}_{\bar{j}^n-1}^{n+1} &= \frac{\alpha^{n+1} A_{\bar{j}^n-1}}{\alpha^{n+1} A_{\bar{j}^n-1} + A_{\bar{j}^n} + A_{\bar{j}^n+1}} \mathbf{m}_{\bar{j}^n}^{C,n+1}, \\ A_{\bar{j}^n} \mathbf{C}_{\bar{j}^n}^{n+1} &= \frac{A_{\bar{j}^n}}{\alpha^{n+1} A_{\bar{j}^n-1} + A_{\bar{j}^n} + A_{\bar{j}^n+1}} \mathbf{m}_{\bar{j}^n}^{C,n+1}, \\ A_{\bar{j}^n+1} \mathbf{C}_{\bar{j}^n+1}^{n+1} &= \frac{A_{\bar{j}^n+1}}{\alpha^{n+1} A_{\bar{j}^n-1} + A_{\bar{j}^n} + A_{\bar{j}^n+1}} \mathbf{m}_{\bar{j}^n}^{C,n+1}. \end{aligned}$$

Fill case $\bar{j}^n = \bar{j}^{n+1} - 1$, Figure 3 (c): The surface moves downwards and crosses a cell boundary. All the mass ends up in one cell: $A_{\bar{j}^n+1} \mathbf{C}_{\bar{j}^n+1}^{n+1} = \mathbf{m}_{\bar{j}^n}^{C,n+1}$.

Cells near the surface during extraction ($t \in T_e$). During extraction, the surface necessarily moves downwards. The initial mass is (35) and the balance law on a red trapezoid (Figures 3 (e) and (f)) gives $\mathbf{m}_{\bar{j}^n}^{C,n+1} = \mathbf{m}_{\bar{j}^n}^{C,n} + \kappa \Psi_{\bar{j}^n}^{C,n}$, where

$$\Psi_{\bar{j}^n}^{C,n} := \Phi_{\bar{j}^n+1/2}^{C,n} - \Phi_{\bar{j}^n+3/2}^{C,n} + h(A_{\bar{j}^n} \mathbf{R}_{\mathbf{C},\bar{j}^n}^n + A_{\bar{j}^n+1} \mathbf{R}_{\mathbf{C},\bar{j}^n+1}^n). \quad (39)$$

Extraction case $\bar{j}^n = \bar{j}^{n+1} - 1$, Figure 3 (e): All the mass ends up in one cell: $A_{\bar{j}^n+1} \mathbf{C}_{\bar{j}^n+1}^{n+1} = \mathbf{m}_{\bar{j}^n}^{C,n+1}$.

Extraction case $\bar{j}^n = \bar{j}^{n+1}$, Figure 3 (f): The surface stays in one cell and we distribute the mass $\mathbf{m}_{\bar{j}^n}^{C,n+1}$ into two cells with (38).

The cell in the extraction pipe. The conservation law for the cell on the x -axis gives the mass equality (Figure 3 (e))

$$A_e \Delta x \mathbf{C}_e^{n+1} = A_e \Delta x \mathbf{C}_e^n + \tau(-Q_e^n \mathbf{C}_e^n - \Phi_{\bar{j}^n+1/2}^{C,n}),$$

where the cross-sectional area A_e of the effluent pipe is of less importance, since we are only interested in \mathbf{C}_e^n and may choose any Δx ; we set $A_e \Delta x := A_1 h$.

3.4. Explicit fully discrete scheme. Given data at t_n and the values \bar{z}^{n+1} and \bar{j}^{n+1} , the update formulas for the particulate concentrations are given here and we distinguish between fill and extraction. We define $\lambda_j := \kappa/A_j = \tau/(A_j h)$ and

$$\begin{aligned} T_e^{\text{num}} &:= \{t_n : Q_e^n > 0, Q_f^n = 0\}, & \eta^{n+1} &:= \frac{A_{\bar{j}^n}}{\alpha^{n+1} A_{\bar{j}^n} + A_{\bar{j}^n+1}}, \\ T_f^{\text{num}} &:= \{t_n : Q_e^n = 0, Q_f^n \geq 0\}, & \theta^{n+1} &:= \frac{A_{\bar{j}^n}}{\alpha^{n+1} A_{\bar{j}^n-1} + A_{\bar{j}^n} + A_{\bar{j}^n+1}}. \end{aligned}$$

Scheme during fill. If $t_n \in T_e^{\text{num}}$, then $\mathbf{C}_e^{n+1} = \mathbf{0}$. We compute the numerical flux (33), the fluxes and sources in $\Psi_{f,\bar{j}^n}^{C,n}$ with (37) and

$$\begin{aligned} \mathbf{r}_{f,\bar{j}^n}^{C,n} &:= \mathbf{C}_{\bar{j}^n}^n + (A_{\bar{j}^n+1}/A_{\bar{j}^n})\mathbf{C}_{\bar{j}^n+1}^n + \lambda_{\bar{j}^n}\Psi_{f,\bar{j}^n}^{C,n}, \\ \mathbf{C}_j^{n+1} &= \begin{cases} \alpha^{n+1}\theta^{n+1}\mathbf{r}_{f,\bar{j}^n}^{C,n} & \text{for } j = \bar{j}^n - 1 \text{ and } \bar{j}^n = \bar{j}^{n+1} + 1, \\ \alpha^{n+1}\eta^{n+1}\mathbf{r}_{f,\bar{j}^n}^{C,n} & \text{for } j = \bar{j}^n \text{ and } \bar{j}^n = \bar{j}^{n+1}, \\ \theta^{n+1}\mathbf{r}_{f,\bar{j}^n}^{C,n} & \text{for } j = \bar{j}^n, \bar{j}^n + 1 \text{ and } \bar{j}^n = \bar{j}^{n+1} + 1, \\ (A_{\bar{j}^n}/A_{\bar{j}^n+1})\mathbf{r}_{f,\bar{j}^n}^{C,n} & \text{for } j = \bar{j}^n + 1 \text{ and } \bar{j}^n = \bar{j}^{n+1} - 1, \\ \eta^{n+1}\mathbf{r}_{f,\bar{j}^n}^{C,n} & \text{for } j = \bar{j}^n + 1 \text{ and } \bar{j}^n = \bar{j}^{n+1}, \\ \mathbf{C}_j^n - \lambda_j[\Delta\Phi^C]_j^n + \tau\mathbf{R}_{C,j}^n & \text{for } j = \bar{j}^n + 2, \dots, N, \\ \mathbf{0} & \text{otherwise.} \end{cases} \end{aligned}$$

Scheme during extraction. If $t_n \in T_e^{\text{num}}$, then we compute the flux (34), the fluxes and sources in $\Psi_{e,\bar{j}^n}^{C,n}$ with (39) and

$$\begin{aligned} \mathbf{r}_{e,\bar{j}^n}^{C,n} &:= \mathbf{C}_{\bar{j}^n}^n + (A_{\bar{j}^n+1}/A_{\bar{j}^n})\mathbf{C}_{\bar{j}^n+1}^n + \lambda_{\bar{j}^n}\Psi_{e,\bar{j}^n}^{C,n}, \\ \mathbf{C}_j^{n+1} &= \begin{cases} \alpha^{n+1}\eta^{n+1}\mathbf{r}_{e,\bar{j}^n}^{C,n} & \text{for } j = \bar{j}^n \text{ and } \bar{j}^n = \bar{j}^{n+1}, \\ (A_{\bar{j}^n}/A_{\bar{j}^n+1})\mathbf{r}_{e,\bar{j}^n}^{C,n} & \text{for } j = \bar{j}^n + 1 \text{ and } \bar{j}^n = \bar{j}^{n+1} - 1, \\ \eta^{n+1}\mathbf{r}_{e,\bar{j}^n}^{C,n} & \text{for } j = \bar{j}^n + 1 \text{ and } \bar{j}^n = \bar{j}^{n+1}, \\ \mathbf{C}_j^n - \lambda_j[\Delta\Phi^C]_j^n + \tau\mathbf{R}_{C,j}^n & \text{for } j = \bar{j}^n + 2, \dots, N, \\ \mathbf{0}, & \text{otherwise,} \end{cases} \\ \mathbf{C}_e^{n+1} &= \mathbf{C}_e^n - \lambda_1(Q_e^n\mathbf{C}_e^n + \Phi_{e,\bar{j}^n+1/2}^{C,n}). \end{aligned}$$

Other concentrations. At every time point t_n we have

$$\mathbf{C}_u^{n+1} = \mathbf{C}_u^n + \lambda_{N+1}(\Phi_{N+1/2}^{C,n} - Q_u^n\mathbf{C}_u^n). \quad (40)$$

The analogue formulas for the soluble concentrations \mathbf{S} are obtained by replacing \mathbf{C} by \mathbf{S} and using the corresponding fluxes defined in (27) and (34). Then one computes

$$X_j^n = C_j^{(1),n} + \dots + C_j^{(k_C),n}, \quad W_j^n = \rho_L(1 - X_j^n/\rho_X) - (S_j^{(1),n} + \dots + S_j^{(k_S),n}).$$

3.5. An invariant-region property. It is desirable that the solution vectors $\mathbf{U} := (\mathbf{C}, \mathbf{S})$ and $\mathbf{U}_e := (\mathbf{C}_e, \mathbf{S}_e)$ of the model (1), (23) stay in the set

$$\Omega := \{\mathbf{U} \in \mathbb{R}^{k_C+k_S} : 0 \leq \mathbf{C} \leq \hat{X}, 0 \leq C^{(1)} + \dots + C^{(k_C)} \leq \hat{X}, \mathbf{S} \geq 0\}.$$

To prove that Ω is an invariant set for the numerical solutions of the scheme in Section 3.4, the time step τ has to be bounded. The CFL condition is

$$\tau \max\{\beta_1, \beta_2\} \leq 1, \quad (\text{CFL})$$

where the constants β_1 and β_2 depend on h , h^2 , and the constitutive functions by

$$\begin{aligned} \beta_1 &:= \frac{\|Q\|_T}{A_{\min}h} + \frac{M_1}{h}(\|v'_{\text{hs}}\|\hat{X} + v_{\text{hs}}(0)) + \frac{2M_2}{h^2}(\|d\|\hat{X} + D(\hat{X})) + \max\{M_C, \tilde{M}_C\}, \\ \beta_2 &:= \max\{M_1, 1\} \frac{\rho_X + \hat{X}}{\rho_X - \hat{X}} \frac{\|Q\|_T}{A_{\min}h} + \frac{\hat{X}M_1}{\rho_X - \hat{X}} \frac{2v_{\text{hs}}(0)}{h} + \frac{\hat{X}M_2}{\rho_X - \hat{X}} \frac{D(\hat{X})}{h^2} + M_S, \end{aligned}$$

where the constants are given by (here, ξ represents v_{hs} , v'_{hs} or d)

$$M_C := \sup_{\substack{\mathbf{U} \in \Omega, \\ 1 \leq k \leq k_C}} \left| \frac{\partial R_C^{(k)}}{\partial C^{(k)}} \right|, \quad \tilde{M}_C := \sup_{\substack{\mathbf{U} \in \Omega, \\ 1 \leq k \leq k_C}} \left| \frac{\partial \tilde{R}_C^{(k)}}{\partial C^{(k)}} \right|, \quad M_S := \sup_{\substack{\mathbf{U} \in \Omega, \\ 1 \leq k \leq k_S}} \left| \frac{\partial R_S^{(k)}}{\partial S^{(k)}} \right|,$$

$$\|\xi\| := \max_{0 \leq X \leq \hat{X}} |\xi(X)|, \quad \|Q\|_T := \max_{0 \leq t \leq T} \{|Q_u(t) - Q_f(t)|, Q_u(t) + Q_e(t)\},$$

$$M_1 := \max_{j=1,\dots,N} \left\{ \frac{A_{j+1/2}}{A_j}, \frac{A_{j-1/2}}{A_j} \right\}, \quad M_2 := \max_{j=1,\dots,N} \left\{ \frac{A_{j+1/2} + A_{j-1/2}}{A_j} \right\}.$$

Theorem 1. *If $\mathbf{U}_j^n := (\mathbf{C}_j^n, \mathbf{S}_j^n) \in \Omega$ for all $j \neq \bar{j}^n$, $\bar{\mathbf{U}}_{\bar{j}^n}^n := (\bar{\mathbf{C}}_{\bar{j}^n}^n, \bar{\mathbf{S}}_{\bar{j}^n}^n) \in \Omega$, $\mathbf{U}_e^n := (\mathbf{C}_e^n, \mathbf{S}_e^n) \in \Omega$ and (CFL) holds, then $\mathbf{U}_j^{n+1}, \bar{\mathbf{U}}_{\bar{j}^n}^{n+1}, \mathbf{U}_e^{n+1} \in \Omega$.*

The theorem is proved by the following three lemmas and by the fact that (CFL) implies (28), which we have used in the derivation of the scheme.

Lemma 1. *If $\mathbf{U}_j^n := (\mathbf{C}_j^n, \mathbf{S}_j^n) \in \Omega$ for all $j \neq \bar{j}^n$, $\bar{\mathbf{U}}_{\bar{j}^n}^n := (\bar{\mathbf{C}}_{\bar{j}^n}^n, \bar{\mathbf{S}}_{\bar{j}^n}^n) \in \Omega$, $\mathbf{U}_e^n := (\mathbf{C}_e^n, \mathbf{S}_e^n) \in \Omega$ and (CFL) holds, then $0 \leq X_j^{n+1}, \bar{X}_{\bar{j}^n}^{n+1} \leq \hat{X}$ for all j .*

Proof. We write the update formulas as $C_j^{(k),n+1} = \mathcal{H}_{\mathbf{C},j}^{n,(k)}(\mathbf{C}_{j-1}^n, \dots, \mathbf{C}_{j+3}^n)$ for one component $k \in \{1, \dots, k_{\mathbf{C}}\}$ (see Section 3.4). Summing for fixed j all components of the update formula for \mathbf{C}_j^{n+1} one gets a scalar update formula which is equal to the one for component k when the vector $\mathbf{R}_{\mathbf{C},j}^n$ is replaced by the scalar $\tilde{R}_{\mathbf{C},j}^n$. This formula, namely $X_j^{n+1} = \mathcal{H}_{X,j}^n(X_{j-1}^n, \dots, X_{j+3}^n)$, includes for $j = N+1$ the underflow concentrations (40). For the update formulas away from the moving surface, we refer [5, Theorem 3.1] from which we also collect

$$v_{j+1/2}^{X,n,+} = (q_{j+1/2}^n + \gamma_{j+1/2}(v_{\text{hs}}(X_{j+1}^n) - J_{j+1/2}^{\mathbf{C},n}))^+ \leq Q_u^n/A_{j+1/2} + v_{\text{hs}}(0) + \frac{D(\hat{X})}{h}.$$

To show the monotonicity for the cells near the surface, we set

$$\chi^+ := \chi_{\{v_{j+1/2}^{X,n} \geq 0\}}, \quad \chi^- := \chi_{\{v_{j+1/2}^{X,n} \leq 0\}}, \quad \chi_e^- := \chi_{\{v_{e,\bar{j}^n+1/2}^{X,n} \leq 0\}},$$

$$\nu_1 := \hat{X} \left(\frac{\|d\|}{h} + v_{\text{hs}}(0) \right) + \frac{D(\hat{X})}{h}, \quad \nu_2 := \hat{X} \left(\frac{\|d\|}{h} + \|v'_{\text{hs}}\| \right) + \frac{D(\hat{X})}{h},$$

and calculate (where the scalar $\Phi_{j+1/2}^{\mathbf{C},n}$ is the sum of all components of $\Phi_{j+1/2}^{\mathbf{C},n}$; similarly for other vectors)

$$\frac{\partial v_{j+1/2}^{X,n,\pm}}{\partial X_j^n} = \chi^\pm \frac{d(X_j^n)}{h}, \quad \frac{\partial v_{j+1/2}^{X,n,\pm}}{\partial X_{j+1}^n} = v'_{\text{hs}}(X_{j+1}^n) - \chi^\pm \frac{d(X_{j+1}^n)}{h},$$

$$\frac{\partial \Phi_{j+1/2}^{\mathbf{C},n}}{\partial X_j^n} = A_{j+1/2} \left((\chi^- X_{j+1}^n + \chi^+ X_j^n) \frac{d(X_j^n)}{h} + v_{j+1/2}^{X,n,+} \right) \leq A_{j+1/2} \nu_1 + Q_u^n,$$

$$\frac{\partial \Phi_{j+1/2}^{\mathbf{C},n}}{\partial X_{j+1}^n} = A_{j+1/2} \left(v_{j+1/2}^{X,n,-} + (\chi^- X_{j+1}^n + \chi^+ X_j^n) \left(v'_{\text{hs}}(X_{j+1}^n) - \frac{d(X_{j+1}^n)}{h} \right) \right) \leq 0,$$

$$\frac{\partial \Psi_{f,j}^{\mathbf{C},n}}{\partial X_{j-1}^n} = 0, \quad \frac{\partial \Psi_{f,j}^{\mathbf{C},n}}{\partial X_j^n} = h A_j \frac{\partial \tilde{R}_{\mathbf{C},j}^n}{\partial X_j^n} \geq -A_j h \tilde{M}_{\mathbf{C}},$$

$$\frac{\partial \Psi_{f,j}^{\mathbf{C},n}}{\partial X_{j+1}^n} = -\frac{\partial \Phi_{j+3/2}^{\mathbf{C},n}}{\partial X_{j+1}^n} + h A_{j+1} \frac{\partial \tilde{R}_{\mathbf{C},j+1}^n}{\partial X_{j+1}^n} \geq -A_{j+3/2} \nu_1 - Q_u^n - A_{j+1} h \tilde{M}_{\mathbf{C}},$$

$$\frac{\partial \Psi_{f,j}^{\mathbf{C},n}}{\partial X_{j+2}^n} = -\frac{\partial \Phi_{j+3/2}^{\mathbf{C},n}}{\partial X_{j+2}^n} \geq 0.$$

In the case $t_n \in T_f^{\text{num}}$, all the coefficients for $\Upsilon_{f,j^n}^{\mathbf{C},n}$ are positive, so it suffices to show that the derivatives of this function are positive under (CFL):

$$\frac{\partial \Upsilon_{f,j}^{\mathbf{C},n}}{\partial X_{j-1}^n} = \lambda_j \frac{\partial \Psi_{f,j}^{\mathbf{C},n}}{\partial X_{j-1}^n} = 0, \quad \frac{\partial \Upsilon_{f,j}^{\mathbf{C},n}}{\partial X_{j+2}^n} = \lambda_j \frac{\partial \Psi_{f,j}^{\mathbf{C},n}}{\partial X_{j+2}^n} \geq 0,$$

$$\begin{aligned}
\frac{\partial \Upsilon_{f,j}^{C,n}}{\partial X_j^n} &= 1 + \lambda_j \frac{\partial \Psi_{f,j}^{C,n}}{\partial X_j^n} \geq 1 - \lambda_j (A_j h \tilde{M}_C) = 1 - \tau \tilde{M}_C \geq 0, \\
\frac{\partial \Upsilon_{f,j}^{C,n}}{\partial X_{j+1}^n} &= \frac{A_{j+1}}{A_j} + \lambda_j \frac{\partial \Psi_{f,j}^{C,n}}{\partial X_{j+1}^n} \geq \frac{A_{j+1}}{A_j} - \lambda_j (A_{j+3/2} \nu_1 + Q_u^n + A_{j+1} h \tilde{M}_C) \\
&\geq A_{j+1}/A_j \left(1 - \tau \left(\frac{M_1 \nu_1}{h} + \frac{\|Q\|_T}{A_{\min} h} + \tilde{M}_C \right) \right) \geq 0.
\end{aligned}$$

In the case $t_n \in T_e^{\text{num}}$, we first estimate

$$\begin{aligned}
\frac{\partial \Phi_{e,j+1/2}^{C,n}}{\partial X_{j+1}^n} &= A_{j+1/2} \left(\chi_e^- \left(v'_{\text{hs}}(X_{j+1}^n) - \frac{d(X_{j+1}^n)}{h} \right) X_{j+1} + v_{e,j+1/2}^{X,n,-} \right) \\
&\geq -A_{j+1/2} \nu_2 - Q_e^n.
\end{aligned}$$

This estimation shall be added to the derivatives of $\Psi_{f,j}^{C,n}$ to obtain those for $\Psi_{e,j}^{C,n}$. The only derivative that differs from those above is

$$\begin{aligned}
\frac{\partial \Upsilon_{e,j}^{C,n}}{\partial X_{j+1}^n} &= \frac{A_{j+1}}{A_j} + \lambda_j \frac{\partial \Psi_{e,j}^{C,n}}{\partial X_{j+1}^n} \\
&\geq \frac{A_{j+1}}{A_j} - \lambda_j (A_{j+1/2} \nu_2 + Q_e^n + A_{j+3/2} \nu_1 + Q_u^n + A_{j+1} h \tilde{M}_C) \\
&\geq \frac{A_{j+1}}{A_j} \left(1 - \tau \left(\frac{M_1(\nu_1 + \nu_2)}{h} + \frac{\|Q\|_T}{A_{\min} h} + \tilde{M}_C \right) \right) \geq 0.
\end{aligned}$$

Next, we write $C_e^{n+1,(k)} = \mathcal{H}_{C_e}^{(k)}(C_e^n, C_{\bar{j}^{n+1}}^n)$ for the update formula for one component (they are all equal) of the effluent concentration. Summing all the components, we obtain $X_e^{n+1} = \mathcal{H}_{C_e}^{(k)}(X_e^n, X_{\bar{j}^{n+1}}^n)$ for any fixed $k \in \{1, \dots, k_C\}$. This formula is trivial for $t_n \in T_f^{\text{num}}$, and for $t_n \in T_e^{\text{num}}$, we get

$$\frac{\partial \mathcal{H}_{C_e}^{(k)}}{\partial X_e^n} = 1 - \lambda_1 Q_e^n \geq 1 - \tau \frac{\|Q\|_T}{A_{\min} h} \geq 0, \quad \frac{\partial \mathcal{H}_{C_e}^{(k)}}{\partial X_{\bar{j}^{n+1}}^n} = -\lambda_1 \frac{\partial \Phi_{e,j+1/2}^{C,n}}{\partial X_{j+1}^n} \geq 0.$$

To prove the boundedness, the monotonicity in each variable of $\mathcal{H}_{X,j}^n$ and the assumptions (3) and (4) are used to obtain, for $t_n \in T_f^{\text{num}}$ and $j = \bar{j}^n = \bar{j}^{n+1}$,

$$\begin{aligned}
0 &\leq \alpha^{n+1} \eta_j^{n+1} \lambda_j Q_f^n X_f^n = \mathcal{H}_{X,j}^n(0, \dots, 0) \leq X_j^{n+1} = \mathcal{H}_{X,j}^n(0, X_j^n, \dots, X_{j+3}^n) \\
&\leq \mathcal{H}_{X,j}^n(0, \alpha^n \hat{X}, \hat{X}, \hat{X}, \hat{X}) = \alpha^{n+1} \eta_j^{n+1} (\alpha^n \hat{X} + (A_{j+1}/A_j) \hat{X} + \lambda_j (Q_f^n X_f^n - Q_u^n \hat{X})) \\
&\leq \alpha^{n+1} \eta_j^{n+1} \hat{X} (\alpha^n + A_{j+1}/A_j + \lambda_j (Q_f^n - Q_u^n)) \\
&\stackrel{(31)}{=} \alpha^{n+1} \hat{X} \eta_j^{n+1} (A_{j+1}/A_j + \alpha^{n+1}) = \alpha^{n+1} \hat{X}.
\end{aligned}$$

For $t_n \in T_f^{\text{num}}$ and $j = \bar{j}^n - 1 = \bar{j}^{n+1}$, we first see that (30) implies; cf. Figure 3(b),

$$\alpha^{n+1} A_{\bar{j}^n-1} + A_{\bar{j}^n} - \alpha^n A_{\bar{j}^n} = (Q_f^n - Q_u^n) \kappa, \tag{41}$$

which we use at the end of the following estimate:

$$\begin{aligned}
0 &\leq \alpha^{n+1} \theta^{n+1} \lambda_{\bar{j}^n-1} Q_f X_f^n = \mathcal{H}_{X,\bar{j}^n-1}^n(0, \dots, 0) \leq X_{\bar{j}^n-1}^{n+1} = X_{\bar{j}^n+1}^{n+1} \\
&= \mathcal{H}_{X,\bar{j}^n-1}^n(0, 0, X_{\bar{j}^n}^n, X_{\bar{j}^n+1}^n, X_{\bar{j}^n+2}^n) \leq \mathcal{H}_{X,\bar{j}^n-1}^n(0, 0, \alpha^n \hat{X}, \hat{X}, \hat{X}) \\
&= \alpha^{n+1} \theta^{n+1} (\alpha^n \hat{X} + (A_{\bar{j}^n+1}/A_{\bar{j}^n}) \hat{X} + \lambda_{\bar{j}^n} (Q_f^n X_f^n - Q_u^n \hat{X})) \\
&\leq \alpha^{n+1} \hat{X} \theta^{n+1} (\alpha^n + A_{\bar{j}^n+1}/A_{\bar{j}^n} + \alpha^{n+1} A_{\bar{j}^n-1}/A_{\bar{j}^n} + 1 - \alpha^n) = \alpha^{n+1} \hat{X}.
\end{aligned}$$

In the case $j = \bar{j}^n = \bar{j}^{n+1} + 1$ (cf. Figure 3 (b)) we can still use (41) to obtain

$$\begin{aligned} 0 &\leq \theta^{n+1} \lambda_{\bar{j}^n} Q_f X_f^n = \mathcal{H}_{X, \bar{j}^n}^n(0, \dots, 0) \leq X_{\bar{j}^n}^{(k), n+1} = X_{\bar{j}^{n+1}+1}^{(k), n+1} \\ &= \mathcal{H}_{X, \bar{j}^n}^n(0, 0, X_{\bar{j}^n}^n, X_{\bar{j}^n+1}^n, X_{\bar{j}^n+2}^n) \leq \mathcal{H}_{X, \bar{j}^n}^n(0, 0, \alpha^n \hat{X}, \hat{X}, \hat{X}) \\ &= \theta^{n+1} (\alpha^n \hat{X} + (A_{\bar{j}^n+1}/A_{\bar{j}^n}) \hat{X} + \lambda_{\bar{j}^n} (Q_f^n X_f^n - Q_u^n \hat{X})) \\ &\leq \hat{X} \theta^{n+1} (\alpha^n + A_{\bar{j}^n+1}/A_{\bar{j}^n} + \alpha^{n+1} A_{\bar{j}^n-1}/A_{\bar{j}^n} + 1 - \alpha^n) = \hat{X}. \end{aligned}$$

A similar estimation can be made for the case $j = \bar{j}^n + 1 = \bar{j}^{n+1} + 2$. For the case $j = \bar{j}^n + 1 = \bar{j}^{n+1}$; see Figure 3(c), we note that (30) implies

$$\alpha^{n+1} A_{\bar{j}^n+1} - (\alpha^n A_{\bar{j}^n} + A_{\bar{j}^n+1}) = (Q_f^n - Q_u^n) \kappa,$$

which we use to estimate

$$\begin{aligned} 0 &\leq (A_{\bar{j}^n}/A_{\bar{j}^n+1}) \lambda_{\bar{j}^n} Q_f X_f^n = \mathcal{H}_{X, \bar{j}^n+1}^n(0, \dots, 0) \leq X_{\bar{j}^n+1}^{n+1} = X_{\bar{j}^{n+1}}^{(k), n+1} \\ &= \mathcal{H}_{X, \bar{j}^n+1}^n(0, X_{\bar{j}^n}^n, \dots, X_{\bar{j}^n+3}^n) \leq \mathcal{H}_{X, \bar{j}^n+1}^n(0, \alpha^n \hat{X}, \hat{X}, \hat{X}, \hat{X}) \\ &= (A_{\bar{j}^n}/A_{\bar{j}^n+1}) (\alpha^n \hat{X} + (A_{\bar{j}^n+1}/A_{\bar{j}^n}) \hat{X} + \lambda_{\bar{j}^n} (Q_f^n X_f^{(k), n} - Q_u^n \hat{X})) \\ &\leq (A_{\bar{j}^n}/A_{\bar{j}^n+1}) \hat{X} (\alpha^n + A_{\bar{j}^n+1}/A_{\bar{j}^n} + \alpha^{n+1} A_{\bar{j}^n+1}/A_{\bar{j}^n} - (\alpha^n + A_{\bar{j}^n+1}/A_{\bar{j}^n})) \\ &= \alpha^{n+1} \hat{X}. \end{aligned}$$

The remaining fill cases are similar; we omit details. For $t_n \in T_e^{\text{num}}$, similar estimations apply; the only difference is that $Q_f X_f^{(k), n}$ is replaced by $\Phi_{e, j+1/2}^{C, n}$, which equals zero when the concentrations are zero, to prove the lower bound. For the upper bound, one uses (30) with $\bar{Q}^n = -Q_e^n$ instead of Q_f^n . For the effluent, we get

$$\begin{aligned} 0 &= \mathcal{H}_{C_e}^{(k)}(0, 0) \leq X_e^{(k), n+1} = \mathcal{H}_{C_e}^{(k)}(X_e^n, X_{j^{n+1}}^n) \leq \mathcal{H}_{C_e}^{(k)}(\hat{X}, \hat{X}) \\ &= \hat{X} - \lambda_1 (Q_e^n + Q_u^n) \hat{X} \leq \hat{X}. \end{aligned}$$

□

Lemma 2. If $\mathcal{U}_j^n := (C_j^n, S_j^n) \in \Omega$ for all $j \neq \bar{j}^n$, $\bar{\mathcal{U}}_{\bar{j}^n}^n := (\bar{C}_{\bar{j}^n}^n, \bar{S}_{\bar{j}^n}^n) \in \Omega$, $\mathcal{U}_e^n := (C_e^n, S_e^n) \in \Omega$ and (CFL) holds, then $0 \leq C_j^{n+1}, \bar{C}_{\bar{j}^n}^{n+1}, C_e^{n+1} \leq \hat{X}$ for all j .

Proof. This follows directly, since each component of the update formula for C_j^n is equal to that of X_j^n if $\bar{R}_{C, j}^n$ is replaced in the latter by $R_{C, j}^{n, (k)}$. □

Lemma 3. If $\mathcal{U}_j^n := (C_j^n, S_j^n) \in \Omega$ for all $j \neq \bar{j}^n$, $\bar{\mathcal{U}}_{\bar{j}^n}^n := (\bar{C}_{\bar{j}^n}^n, \bar{S}_{\bar{j}^n}^n) \in \Omega$, $\mathcal{U}_e^n := (C_e^n, S_e^n) \in \Omega$ and (CFL) holds, then $S_j^{n+1} \geq 0$ for all j and $S_e^{n+1} \geq 0$.

Proof. We start as in the proof of Lemma 1, use notation and estimations from there, and prove monotonicity of each component of the right-hand side $\mathcal{H}_{S, j^n}^{n, (k)}$ of the update formula for component $S_j^{n, (k)}$, which we write as S_j^n . We also skip the superscript (k) for components of other vectors. We let $\hat{\rho} := 1/(\rho_X - \hat{X})$ and

$$\nu_3 := \hat{\rho} \left((\rho_X + \hat{X}) \frac{\|Q\|_T}{A_{\min}} + \left(v_{\text{hs}}(0) + \frac{D(\hat{X})}{h} \right) \hat{X} \right).$$

The numerical fluxes are different and we get

$$\begin{aligned} \frac{\partial \Phi_{j+1/2}^{S, n}}{\partial S_j^n} &= A_{j+1/2} \frac{(\rho_X q_{j+1/2}^n - F_{j+1/2}^{X, n})^+}{\rho_X - X_j^n} \leq A_{j+1/2} \hat{\rho} (\rho_X q_{j+1/2}^n - v_{j+1/2}^{X, n, -} \hat{X}) \\ &= A_{j+1/2} \hat{\rho} (\rho_X q_{j+1/2}^n + v_{j+1/2}^{X, n, +} \hat{X}) \\ &\leq A_{j+1/2} \hat{\rho} \left(\rho_X q_{j+1/2}^n + \left(q_{j+1/2}^n + v_{\text{hs}}(0) + \frac{D(\hat{X})}{h} \right) \hat{X} \right) \leq A_{j+1/2} \nu_3, \end{aligned}$$

$$\frac{\partial \Phi_{j+1/2}^{S,n}}{\partial S_{j+1}^n} = A_{j+1/2} \frac{(\rho_X q_{j+1/2}^n - F_{j+1/2}^{X,n})^-}{\rho_X - X_{j+1}} \leq 0.$$

Because of the similarities between $\Psi_{f,j}^{C,n}$ and $\Psi_{f,j}^{S,n}$, we only write the difference here:

$$\frac{\partial \Psi_{f,j}^{S,n}}{\partial S_{j+1}^n} = -\frac{\partial \Phi_{j+3/2}^{S,n}}{\partial S_{j+1}^n} + h A_{j+1} \frac{\partial R_{S,j+1}^n}{\partial S_{j+1}^n} \geq -A_{j+3/2} \nu_3 - A_{j+1} h M_S.$$

To prove the monotonicity in the case $t_n \in T_f^{\text{num}}$, we conclude that the estimations are in fact similar to those in the proof of Lemma 2 with the following difference:

$$\frac{\partial \Upsilon_{f,j}^{S,n}}{\partial S_{j+1}^n} \geq \frac{A_{j+1}}{A_j} \left(1 - \tau \left(\frac{M_1 \nu_3}{h} + M_S \right) \right) \geq 0.$$

To prove the monotonicity in the case $t_n \in T_e^{\text{num}}$, we first estimate

$$\begin{aligned} \frac{\partial \Phi_{e,j+1/2}^{S,n}}{\partial S_{j+1}^n} &= \left(-\frac{A_{j+1/2} X_{j+1}^n}{\rho_X - X_{j+1}^n} \left(v_{\text{hs}}(X_{j+1}^n) - \frac{D(X_{j+1}^n)}{h} \right) - Q_e^n \right)^- \\ &\geq -A_{j+1/2} \hat{\rho} \hat{X} v_{\text{hs}}(0) - Q_e^n. \end{aligned}$$

Following the same procedure as in the proof of Lemma 2, we now get

$$\begin{aligned} \frac{\partial \Upsilon_{e,j}^{S,n}}{\partial S_{j+1}^n} &= \frac{A_{j+1}}{A_j} + \lambda_j \frac{\partial \Psi_{e,j}^{S,n}}{\partial S_{j+1}^n} \geq \frac{A_{j+1}}{A_j} - \lambda_j \left\{ A_{j+1/2} \hat{\rho} \hat{X} v_{\text{hs}}(0) + Q_e^n \right. \\ &\quad \left. + \hat{\rho} \left((\rho_X + \hat{X}) Q_u^n + A_{j+3/2} \left(v_{\text{hs}}(0) + \frac{D(\hat{X})}{h} \right) \hat{X} \right) + A_{j+1} h M_S \right\} \\ &\geq \frac{A_{j+1}}{A_j} \left(1 - \tau \left(\frac{M_1 (\hat{\rho} \hat{X} v_{\text{hs}}(0) + \nu_3)}{h} + M_S \right) \right) \geq 0. \end{aligned}$$

For the update of the effluent concentrations, we get the same result for S_e^n as for C_e^n .

The proof of positivity can be done as in the proof of Lemma 2. \square

4. APPLICATION TO SEQUENCING BATCH REACTORS

An SBR cycle consists of five stages; see Figure 2. During some of these periods, mixing may occur due to aeration or the movement of an impeller. For the sake of simplicity, we ignore partial mixing and exemplify the cases of either no mixing or full mixing. The PDE model (26) includes no mixing and we next derive the special case of full mixing.

4.1. Model and numerics during a full mixing react stage. Full mixing means that the relative velocity v_{rel} is negligible. We set $v_{\text{rel}} \equiv 0$ and assume that concentrations only depend on t (below the surface). Then $v_X = v_L = q$, hence,

$$\Phi_C = A(z) q(z, t) C = Q_u(t) \chi_{\{z > \bar{z}(t)\}} C, \quad \Phi_S = Q_u(t) \chi_{\{z > \bar{z}(t)\}} S. \quad (42)$$

Integrating the PDEs (26) from $\bar{z}(t)^-$ to B , one gets the governing ODEs. The integral of the time-derivative term of (26a) can, by means of (20), be written as

$$\begin{aligned} \int_{\bar{z}(t)}^B \frac{dC}{dt} A(\xi) d\xi &= \frac{d}{dt} \int_{\bar{z}(t)}^B C(t) A(\xi) d\xi - (-C(t) A(\bar{z}(t)) \bar{z}'(t)) \\ &= \frac{dC(t)}{dt} \bar{V}(t) - C(t) (Q_u(t) - \bar{Q}(t)). \end{aligned}$$

The spatial-derivative term of (26a) becomes, with (42),

$$\int_{\bar{z}(t)}^B \frac{d\Phi_C}{dz} d\xi = Q_u(t) C(t) - 0.$$

The same can be done for the substrate equations and we obtain the following system of ODEs for the homogeneous concentrations in $\bar{z}(t) < z < B$:

$$\bar{V}(t) \frac{d\mathbf{C}}{dt} = (Q_u(t) - \bar{Q}(t))\mathbf{C} + Q_f(t)\mathbf{C}_f(t) + \bar{V}(t)\mathbf{R}_\mathbf{C}, \quad (43a)$$

$$\bar{V}(t) \frac{d\mathbf{S}}{dt} = (Q_u(t) - \bar{Q}(t))\mathbf{S} + Q_f(t)\mathbf{S}_f(t) + \bar{V}(t)\mathbf{R}_\mathbf{S}, \quad (43b)$$

where all concentrations depend only on time, since they are averages (below the surface). As before, W can be obtained afterwards from (6). In the region $0 < z < \bar{z}(t)$ all concentrations are zero. Because of (10c) and (24), we have $\mathbf{C}_u(t) = \mathbf{C}(t)$ and $\mathbf{C}_e(t) = \mathbf{C}(t)\chi_{\{t \in T_e\}}$ (analogously for \mathbf{S}).

Suppose the PDE solution $\mathbf{C}(z, T_0)$ (or the numerical one) is known at $t = T_0 = t_{n_0}$ when a period of complete mixing starts. The initial concentrations for the ODEs (43) are defined as the averages (for $k = 1, \dots, k_\mathbf{C}$; analogously for \mathbf{S})

$$C^{(k)}(T_0) := \frac{1}{\bar{V}(T_0)} \int_{\bar{z}(T_0)}^B A(\xi) C^{(k)}(\xi, T_0) d\xi \approx \frac{h}{\bar{V}(T_0)} \sum_{i=1}^N A_i C_i^{(k), n_0} =: C_{\text{aver}}^{(k), n_0}.$$

The system (43) thus models a completely stirred tank with reactions, possibly a moving upper boundary because of in- and outflow streams.

If an ODE mixing period ends at $t = T = t_{\bar{n}}$ and the PDE model is to be used thereafter, then the total mass below the surface is distributed among the cells by

$$C_j^{(k), \bar{n}} := \begin{cases} 0 & \text{for } j = 1, \dots, \bar{j}^{\bar{n}} - 1, \\ \alpha^{\bar{n}} C_{\text{aver}}^{(k), \bar{n}} = (z_{\bar{j}^{\bar{n}}+1/2} - \bar{z}^{\bar{n}}) C_{\text{aver}}^{(k), \bar{n}} & \text{for } j = \bar{j}^{\bar{n}}, \\ C_{\text{aver}}^{(k), \bar{n}} & \text{for } j = \bar{j}^{\bar{n}} + 1, \dots, N. \end{cases}$$

5. NUMERICAL EXAMPLES

To exemplify the entire process, we use the same model for denitrification as in [6] with two solid components: ordinary heterotrophic organisms X_{OHO} and undegradable organics X_U ; and three soluble components: nitrate S_{NO_3} , readily biodegradable substrate S_S and nitrogen S_{N_2} . Thus, we utilize $\mathbf{C} = (X_{\text{OHO}}, X_U)^T$ and $\mathbf{S} = (S_{\text{NO}_3}, S_S, S_{\text{N}_2})^T$, corresponding to $k_\mathbf{C} = 2$ and $k_\mathbf{S} = 3$, respectively. Shortly described, the denitrification process converts nitrate (NO_3) to nitrogen gas (N_2) by a series of reactions involving the particulate biomass. The reaction terms for the solid and liquid phases used for all numerical examples are

$$\mathbf{R}_\mathbf{C} = X_{\text{OHO}} Z(X) (\mu(\mathbf{S}) - b, f_P b)^T,$$

$$\mathbf{R}_\mathbf{S} = X_{\text{OHO}} (-\bar{Y} \mu(\mathbf{S}), (1 - f_P) b - \mu(\mathbf{S})/Y, \bar{Y} \mu(\mathbf{S}))^T, \quad \bar{Y} = (1 - Y)/(2.86Y),$$

where $Y = 0.67$ is a yield factor, $b = 6.94 \times 10^{-6} \text{ s}^{-1}$ is the decay rate of heterotrophic organisms and $f_P = 0.2$ is the portion of these that decays to undegradable organics. The continuous function $Z(X)$ must not influence the condition (CFL), be equal to one for most concentration and satisfy $Z(\hat{X}) = 0$ because of the technical assumption (3). We have used $\hat{X} = 30 \text{ kg/m}^3$, a value our simulated solutions never reach, despite we have simulated with $Z(X) \equiv 1$. The growth-rate function

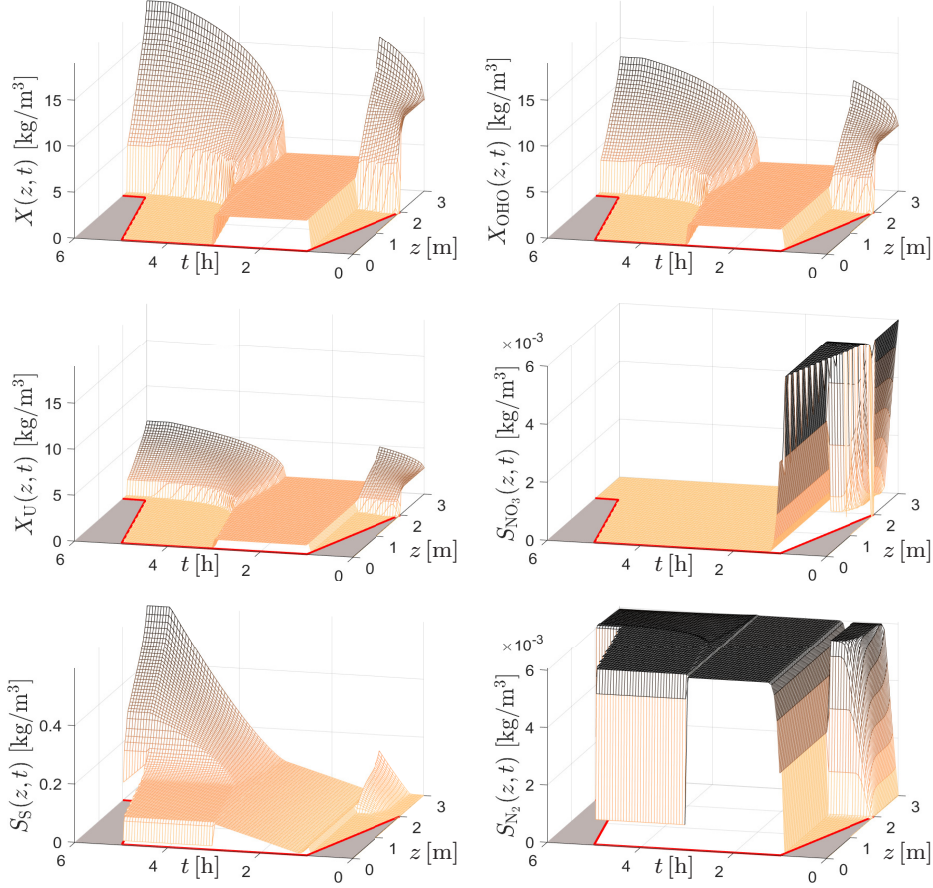
$$\mu(\mathbf{S}) = \mu_{\max} \frac{S_{\text{NO}_3}}{K_{\text{NO}_3} + S_{\text{NO}_3}} \frac{S_S}{K_S + S_S}$$

has the parameters $\mu_{\max} = 5.56 \times 10^{-5} \text{ s}^{-1}$, $K_{\text{NO}_3} = 5 \times 10^{-4} \text{ kg/m}^3$ and $K_S = 0.02 \text{ kg/m}^3$. Adding the components of the reaction terms we get

$$\tilde{\mathbf{R}}_\mathbf{C} = R_\mathbf{C}^{(1)} + R_\mathbf{C}^{(2)} = (\mu(\mathbf{S}) - (1 - f_P) b) X_{\text{OHO}} Z(X), \quad \tilde{\mathbf{R}}_\mathbf{S} = R_\mathbf{S}^{(2)}.$$

Table 1. Example 1: Time functions for an SBR cycle. ‘Model’ refers to either PDE (26) or ODE (43).

Stage	Time period [h]	$Q_f(t)[\text{m}^3/\text{h}]$	$Q_u(t)[\text{m}^3/\text{h}]$	$Q_e(t)[\text{m}^3/\text{h}]$	Model
Fill	$0 \leq t < 1$	790	0	0	PDE
React	$1 \leq t < 3$	0	0	0	ODE
Settle	$3 \leq t < 5$	0	0	0	PDE
Draw	$5 \leq t < 5.5$	0	0	1570	PDE
Idle	$5.5 \leq t < 6$	0	10	0	PDE

**Figure 4.** Example 1: Simulation results (with $N = 100$, $\tau = 6/63498$) during $T = 6$ hours.

The constitutive functions used in all simulations are

$$v_{\text{hs}}(X) := \frac{v_0}{1 + (X/\hat{X})^\eta}, \quad \sigma_e(X) := \alpha \chi_{\{X \geq X_c\}}(X - X_c),$$

with $v_0 = 1.76 \times 10^{-3} \text{ m/s}$, $\hat{X} = 3.87 \text{ kg/m}^3$, $\eta = 3.58$, $X_c = 5 \text{ kg/m}^3$ and $\alpha = 0.2 \text{ m}^2/\text{s}^2$. Other parameters are $\rho_X = 1050 \text{ kg/m}^3$, $\rho_L = 998 \text{ kg/m}^3$, $g = 9.81 \text{ m/s}^2$, and $B = 3 \text{ m}$. The soluble feed concentrations in both examples are

$$\mathbf{S}_f(t) \equiv (6.00 \times 10^{-3}, 9.00 \times 10^{-4}, 0)^T \text{ kg/m}^3. \quad (44)$$

For visualization purposes, we do not plot zero numerical concentrations above the surface, but fill this region with grey color.

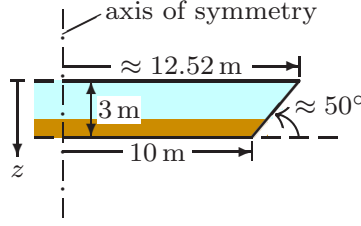


Figure 5. Example 2: Schematic of the truncated cone.

Table 2. Example 2. Schematic of the truncated cone and time functions for the simulation. ‘Model’ refers to either PDE (26) or ODE (43).

Time period [h]	$X_f(t)$ [kg/m ³]	$Q_f(t)$ [m ³ /h]	$Q_u(t)$ [m ³ /h]	$Q_e(t)$ [m ³ /h]	Model
$0 \leq t < 1$	5	790	0	0	PDE
$1 \leq t < 2$	0	0	100	0	ODE
$2 \leq t < 3$	0	0	0	100	ODE
$3 \leq t < 5$	5	100	0	0	PDE
$5 \leq t < 6$	0	0	0	790	PDE

5.1. Example 1: An SBR cycle. A cylindrical tank with cross-sectional area $A = 400 \text{ m}^2$ is simulated during 6 h. The lengths of the five stages are chosen primarily for illustration; see Table 1. The initial concentrations are $\mathbf{C}^0(z) = X^0(z)(5/7, 2/7)^T$, where

$$\begin{aligned} X^0(z) &= 0 \text{ kg/m}^3, \quad \mathbf{S}^0(z) = \mathbf{0} \text{ kg/m}^3 & \text{if } z < 2.0 \text{ m,} \\ X^0(z) &= 10 \text{ kg/m}^3 \quad \mathbf{S}^0(z) = (6 \times 10^{-3}, 9 \times 10^{-4}, 0)^T \text{ kg/m}^3 & \text{if } z \geq 2.0 \text{ m.} \end{aligned}$$

No biomass is fed to the tank; $\mathbf{C}_f(t) \equiv \mathbf{0}$. Figure 4 shows the simulation results. The reactions converting NO_3 to N_2 start immediately and are fast. (The downwards-pointing peaks in the S_{NO_3} plot arise since we do not plot zero concentrations above the surface.) A short time after the react stage has started at $t = 1$ h, all NO_3 has been consumed. During this short time period, S_S decreases slightly when there is still sufficient NO_3 , but then increases during the react stage because of the decay of heterotrophic organisms.

5.2. Example 2. We now choose a truncated cone (cf. Figure 5) of the same volume 1200 m^3 as the cylinder of Example 1 and demonstrate what the numerical scheme can handle during extreme cases of fill and draw when solids concentrations are positive at the surface. We use the same initial data as in Example 1 but with $\bar{z}(0) \approx 1.8429 \text{ m}$ to obtain the same initial volume of mixture as in Example 1. The fill and draw periods are specified in Table 2. The feed concentrations of the substrates are given by (44) and those of the biomass by $\mathbf{C}_f(t) = X_f(t)(5/7, 2/7)^T$, where the piecewise constant function $X_f(t)$ follows from Table 2.

Figure 6 shows the simulated concentrations. During the first hour, there is a discontinuity in the solids concentration X rising with a lower speed than the surface. Then full mixing occurs during two hours and the surface is lowered because of the outlet flows at the bottom and top. At $t = 3$ h, the mixing stops and the solids settle again. During $3 \text{ h} < t < 5 \text{ h}$, the tank is filled up again with solids and substrates. The solids feed concentration $X_f = 5 \text{ kg/m}^3$ is the same as during the first hour, but now the feed flow Q_f is much lower, and hence the mass flow much lower. The results is a very low concentration X below the surface during $3 \text{ h} < t < 5 \text{ h}$. Since also X_{OHO} is low, there are hardly any reactions and most of the fed NO_3 remains in the mixture above the sludge blanket of the solids. At the surface level around $t = 3$ h, there is also biomass present and a high production of N_2 occurs. However, the sludge blanket drops and the high concentration

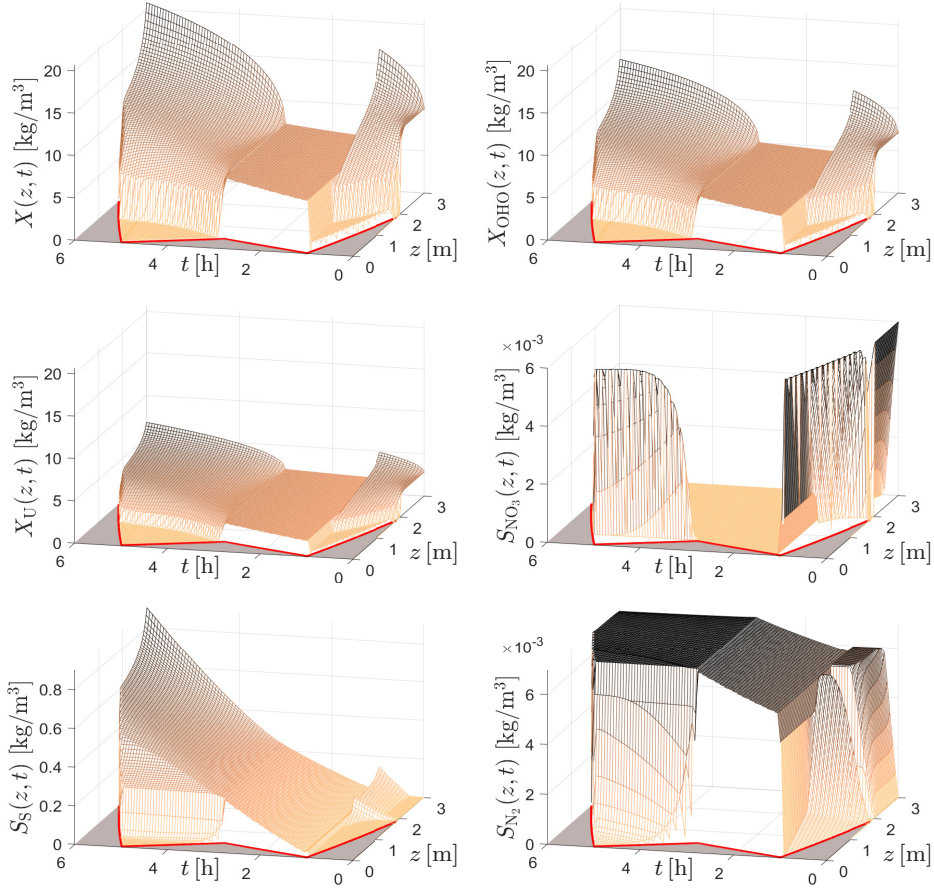


Figure 6. Example 2: Simulated results during $T = 6$ hours.

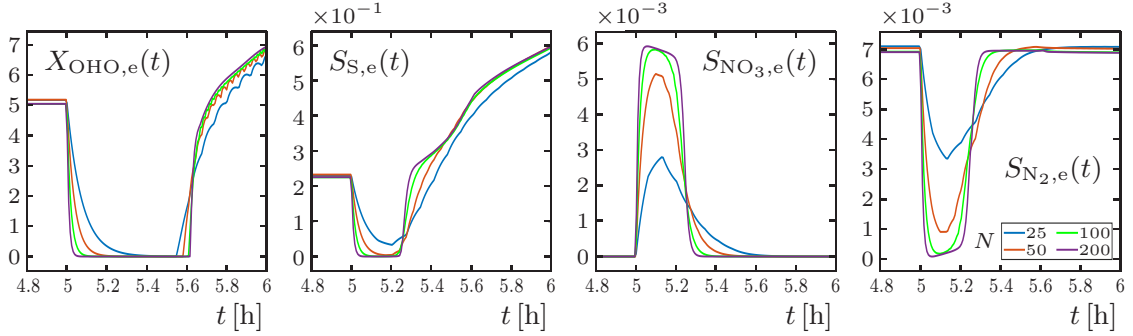


Figure 7. Example 2: Simulated effluent concentrations, all in kg/m^3 , during $t \in [4.8 \text{ h}, 6 \text{ h}]$ obtained by the discretizations (number of cells within the tank) $N = 25, 50, 100$, and 200 .

of N_2 remains at this height until it is extracted through the effluent during the last hour. The latter is shown in Figure 7, which also shows that solids are extracted.

6. CONCLUSIONS

A general model of multi-component reactive settling of flocculated particles given by a quasi-one-dimensional PDE system with moving boundary (1), (23) and a numerical scheme (Section 3.4) for its simulation are introduced. Fill and draw of mixture at the moving surface can be made at any time and a specific application is the SBR process.

The unknowns are concentrations of solids and soluble substrates, and the PDE model can (via its reaction terms) be combined with well-established models for the biochemical reactions in wastewater treatment.

The moving boundary can be precomputed with the ODE (20) containing the volumetric flows in and out of the tank. The numerical scheme is designed to ensure conservation of mass across the surface during fill and draw. The main result is an invariant-region property (Theorem 1) for the numerical solution; all concentrations are nonnegative and the solids concentrations never exceed the maximal packing one. An indication of the convergence of the numerical scheme as the mesh size is reduced is given by the results shown in Figure 7. A proof of convergence of the method (as $h \rightarrow 0$) to a suitably defined weak or entropy weak solution, as well as the corresponding well-posedness (existence and uniqueness) analysis, are still pending. That said, we point out that available convergence analyses for related strongly degenerate, scalar PDEs with discontinuous flux (cf., e.g., [9, 22, 23]) rely on the monotonicity of the underlying scheme as well as a uniform bound on the numerical solution, among other properties. Theorem 1 and its proof may be therefore viewed as a partial result to prove convergence of the numerical scheme presented herein.

Given a moving boundary and a fixed spatial discretization for the numerical scheme, local mass balances have been used to obtain correct update formulas for numerical cells near the surface. This results in a scheme (see Section 3.4) with several cases depending on the surface movement. A certain limitation of the explicit numerical scheme is the restrictive CFL condition (where the time step is proportional to the square of the cell size), implying that very small time steps are needed if accurate approximations on a fine spatial mesh are sought. An alternative approach would be to transform the PDE system and have a fixed number of cells below the moving surface. Such a scheme could possibly also be easier to generalize to a high-order scheme or a more efficient one with semi-implicit time discretization. The advantage of the present fixed-cell-size numerical scheme is, however, that the model can more easily be generalized to include further sources or sinks at fixed locations, a desirable feature in applications to wastewater treatment.

With the present model, investigations and optimization of the SBR process can be made, and the usage of several SBRs coupled in series or in parallel with synchronized stages so that, e.g., a continuous stream of effluent of certain quality is obtained. Furthermore, more accurate comparisons are possible between SBRs and continuously operated SSTs, since one or the other may be preferred depending on the plant size and other practical considerations [16].

ACKNOWLEDGEMENTS

RB is supported by CMM, project ANID/PIA/AFB170001; CRHIAM, project ANID/FONDAP/15130015; and Fondecyt project 1210610. SD acknowledges support from the Swedish Research Council (Vetenskapsrådet, 2019-04601). RP is supported by ANID scholarship ANID-PCHA/Doctorado Nacional/2020-21200939.

REFERENCES

- [1] Adimurthi, J. Jaffré and G. D. V. Gowda, Godunov-type methods for conservation laws with a flux function discontinuous in space, *SIAM J. Numer. Anal.*, 42 (2004) 179–208.
- [2] M. M. Amin, M. H. Khiadani (Hajian), A. Fatehizadeh and E. Taheri, Validation of linear and non-linear kinetic modeling of saline wastewater treatment by sequencing batch reactor with adapted and non-adapted consortiums, *Desalination*, 344 (2014) 228–235.

- [3] B. Andreianov, K. H. Karlsen and N. H. Risebro, A theory of L^1 -dissipative solvers for scalar conservation laws with discontinuous flux, *Arch. Ration. Mech. Anal.*, 201 (2011) 1–60.
- [4] R. Bürger, J. Careaga and S. Diehl, A simulation model for settling tanks with varying cross-sectional area, *Chem. Eng. Commun.*, 204 (2017) 1270–1281.
- [5] R. Bürger, J. Careaga and S. Diehl, A method-of-lines formulation for a model of reactive settling in tanks with varying cross-sectional area, *IMA J. Appl. Math.*, 86 (2021) 514–546.
- [6] R. Bürger, J. Careaga, S. Diehl, C. Mejías, I. Nopens, E. Torfs and P. A. Vanrolleghem, Simulations of reactive settling of activated sludge with a reduced biokinetic model, *Computers Chem. Eng.*, 92 (2016) 216–229.
- [7] R. Bürger, S. Diehl and C. Mejías, A difference scheme for a degenerating convection-diffusion-reaction system modelling continuous sedimentation, *ESAIM: Math. Modelling Numer. Anal.*, 52 (2018) 365–392.
- [8] R. Bürger, S. Diehl and I. Nopens, A consistent modelling methodology for secondary settling tanks in wastewater treatment, *Water Res.*, 45 (2011) 2247–2260.
- [9] R. Bürger, K. H. Karlsen and J. D. Towers, A model of continuous sedimentation of flocculated suspensions in clarifier-thickener units, *SIAM J. Appl. Math.*, 65 (2005) 882–940.
- [10] M. Caluwé, D. Daens, R. Blust, L. Geuens and J. Dries, The sequencing batch reactor as an excellent configuration to treat wastewater from the petrochemical industry, *Water Sci. Tech.*, 75 (2016) 793–801.
- [11] J.-P. Chancelier, M. Cohen de Lara and F. Pacard, Analysis of a conservation PDE with discontinuous flux: a model of settler, *SIAM J. Appl. Math.*, 54 (1994) 954–995.
- [12] G. Chen, M. C. M. van Loosdrecht, G. A. Ekama and D. Brdjanovic, *Biological Wastewater Treatment*, (IWA Publishing, London, UK, second ed., 2020).
- [13] S. Diehl, On scalar conservation laws with point source and discontinuous flux function, *SIAM J. Math. Anal.*, 26 (1995) 1425–1451.
- [14] S. Diehl, A conservation law with point source and discontinuous flux function modelling continuous sedimentation, *SIAM J. Appl. Math.*, 56 (1996) 388–419.
- [15] S. Diehl, Dynamic and steady-state behavior of continuous sedimentation, *SIAM J. Appl. Math.*, 57 (1997) 991–1018.
- [16] R. Droste and R. Gear, *Theory and Practice of Water and Wastewater Treatment*, Wiley, Hoboken, NJ, USA, 2nd ed., 2019.
- [17] E. Freytez, A. Márquez, M. Pire, E. Guevara and S. Perez, Nitrogenated substrate removal modeling in sequencing batch reactor oxic-anoxic phases, *J. Environ. Eng.*, 145 (2019) 04019068.
- [18] P. Gajardo, H. Ramírez and A. Rapaport, Minimal time sequential batch reactors with bounded and impulse controls for one or more species, *SIAM J. Control Optim.*, 47 (2008) 2827–2856.
- [19] T. Gimse and N. H. Risebro, Solution of the Cauchy problem for a conservation law with a discontinuous flux function, *SIAM J. Math. Anal.*, 23 (1992) 635–648.
- [20] M. Henze, Gujer, T. W., Mino and M. C. M. van Loosdrecht, Activated Sludge Models ASM1, ASM2, ASM2d and ASM3, IWA Scientific and Technical Report No. 9, IWA Publishing, London, UK, 2000.
- [21] Z. Hu, R. A. Ferraina, J. F. Ericson, A. A. MacKay and B. F. Smets, Biomass characteristics in three sequencing batch reactors treating a wastewater containing synthetic organic chemicals, *Water Res.*, 39 (2005) 710–720.
- [22] K. H. Karlsen, N. H. Risebro and J. D. Towers, Upwind difference approximations for degenerate parabolic convection-diffusion equations with a discontinuous coefficient, *IMA J. Numer. Anal.*, 22 (2002) 623–664.
- [23] K. H. Karlsen, N. H. Risebro and J. D. Towers, L^1 stability for entropy solutions of

- nonlinear degenerate parabolic convection-diffusion equations with discontinuous coefficients, *Trans. Royal Norwegian Society Sci. Letters (Skr. K. Nor. Vidensk. Selsk.)*, 3 (2003) 49 pp.
- [24] J. Kauder, N. Boes, C. Pasel and J.-D. Herbell, Combining models ADM1 and ASM2d in a sequencing batch reactor simulation, *Chem. Eng. Technol.*, 30 (2007) 1100–1112.
 - [25] Y. Kim, C. Yoo, Y. Kim and I.-B. Lee, Simulation and activated sludge model-based iterative learning control for a sequencing batch reactor, *Environ. Eng. Sci.*, 26 (2009) 661–671.
 - [26] J. Kocijan and N. Hvala, Sequencing batch-reactor control using gaussian-process models, *Bioresource Technol.*, 137 (2013) 340–348.
 - [27] D. Li, H. Z. Yang and X. F. Liang, Application of Bayesian networks for diagnosis analysis of modified sequencing batch reactor, *Adv. Mater. Res.*, 610–613 (2012) 1139–1145.
 - [28] D. Massé, Comprehensive model of anaerobic digestion of swine manure slurry in a sequencing batch reactor, *Water Res.*, 34 (2000) 3087–3106.
 - [29] T. Meadows, M. Weedermann and G. S. K. Wolkowicz, Global analysis of a simplified model of anaerobic digestion and a new result for the chemostat, *SIAM J. Appl. Math.*, 79 (2019) 668–689.
 - [30] L. Metcalf and H. P. Eddy, *Wastewater Engineering. Treatment and Resource Recovery* (McGraw-Hill, New York, USA, 5th ed., 2014).
 - [31] B.-J. Ni, A. Joss and Z. Yuan, Modeling nitrogen removal with partial nitrification and anammox in one flocc-based sequencing batch reactor, *Water Res.*, 67 (2014) 321–329.
 - [32] V. Pambrun, E. Paul and M. Spérandio, Control and modelling of partial nitrification of effluents with high ammonia concentrations in sequencing batch reactor, *Chem. Eng. Processing: Process Intensification*, 47 (2008) 323–329.
 - [33] R. Piotrowski, M. Lewandowski and A. Paul, Mixed integer nonlinear optimization of biological processes in wastewater sequencing batch reactor, *J. Process Control*, 84 (2019) 89–100.
 - [34] T. Popple, J. Williams, E. May, G. Mills and R. Oliver, Evaluation of a sequencing batch reactor sewage treatment rig for investigating the fate of radioactively labelled pharmaceuticals: Case study of propranolol, *Water Res.*, 88 (2016) 83–92.
 - [35] M. Singh and R. K. Srivastava, Sequencing batch reactor technology for biological wastewater treatment: a review, *Asia-Pacific J. Chem. Eng.*, 6 (2010) 3–13.
 - [36] B. Song, Z. Tian, R. van der Weijden, C. Buisman and J. Weijma, High-rate biological selenate reduction in a sequencing batch reactor for recovery of hexagonal selenium, *Water Res.*, 193 (2021) 116855.
 - [37] S. M. Souza, O. Q. F. Araújo and M. A. Z. Coelho, Model-based optimization of a sequencing batch reactor for biological nitrogen removal, *Bioresource Tech.*, 99 (2008) 3213–3223.
 - [38] S. Wang and C. K. Gunsch, Effects of selected pharmaceutically active compounds on treatment performance in sequencing batch reactors mimicking wastewater treatment plants operations, *Water Res.*, 45 (2011) 3398–3406.